J|A|C|S
ARTICLES
Published on Web 01/24/2002

Calix[4]tubes: A New Class of Potassium-Selective Ionophore

Susan E. Matthews,[†] Phillipe Schmitt,[†] Vitor Felix,[‡,§] Michael G. B. Drew,[‡] and Paul D. Beer*[,†]

Contribution from the Inorganic Chemistry Laboratory, Department of Chemistry, University of Oxford, South Parks Road, Oxford OX1 3QR, U.K., and Department of Chemistry, University of Reading, Whiteknights, Reading, Berkshire RG6 6AD, U.K.

Received July 30, 2001

Abstract: A new class of cryptand-like ionophore based on a bis calix[4]arene structure has been developed. These molecules proved highly selective for complexation of potassium over all group I metal cations and barium. A range of symmetric and asymmetric calix[4]tubes featuring either alkyl or phenyl substituents at the upper rim have been synthesized in exceptional yield. Alteration of the calix[4]arene upper rim environment enables fine-tuning of the rate of potassium uptake, which can be evaluated through the conformational change on binding by NMR studies. Selectivity of potassium complexation has been demonstrated using NMR and electrospray mass spectral techniques. Molecular modeling studies, derived from crystallographic data, confirm that the potassium metal cation is complexed via the axial route, passing through the calix[4]arene annulus, and provide evidence for complexation rate and selectivity.

Introduction

The selective recognition and extraction of alkali metals is currently an area of great interest.[1] In particular, the recent elucidation of the structure of the *Streptomyces lividans* potassium channel[2] has enabled research into the structural requirements of ion channels through synthetic mimetics.[3] Calixarenes offer an ideal platform for the design of potassium-selective ionophores due to their rigidity and ease of derivatization.[4] The tetraacetates of 1,3-alternate calix[4]arene[5] and dioxacalix[4]-arene[6] proved selective for complexation of potassium, and the hexaacetate of calix[6]arene[7] has been developed as a blood sensor for potassium. The majority of research has focused on the development of calix[4]crowns incorporating a crown-5 unit and on the different cation specificities of a range of calixarene conformers.[8−10] Of these, the most successful is the 1,3-alternate receptor,[11] which shows higher K^+/Na^+ selectivity than the natural ionophore valinomycin. However, to date, no calixarene-based system shows selectivity for potassium cations over all alkali and alkaline earth metals.

In this paper we report a new class of cryptand-type ionophore, the calix[4]tube, based on a bis calix[4]arene scaffold, which displays exceptional potassium selectivity. A range of symmetric and asymmetric tubes have been synthesized through modification at the calix[4]arene upper rim. Kinetic NMR studies of the complexation properties of these calix[4]tubes show that the rate of potassium can be tuned through this structural alteration, while NMR and electrospray mass spectral techniques show the exceptional selectivity for complexation of potassium to be maintained. Detailed molecular modeling simulations, based on crystal structures of both the free and potassium-complexed calix[4]tubes, demonstrate a preferred *axial* route of entry for the potassium cation passing through the calix[4]arene annulus.[12]

Synthesis

Our receptor design was based on the formation of a cryptand-type structure, in which two calix[4]arene moieties are linked via four ethylene units to provide a rigid arrangement of eight

* To whom correspondence should be addressed. Fax: (+44) 1865 272690. E-mail: paul.beer@chem.ox.ac.uk.
[†] University of Oxford.
[‡] University of Reading.
[§] On sabbatical leave from the Departamento de Quimica, Universidade de Aveiro, P-3810-193 Aveiro, Portugal.

(1) (a) Ikeda, A.; Shinkai, S. *Chem. Rev.* **1997**, *97*, 1713−1734. (b) Beer, P. D.; Gale, P. A.; Chen, Z. *Adv. Phys. Org. Chem.* **1998**, *31*, 1−90. (c) Zhang, X. X.; Izatt, R. M.; Bradshaw, J. S.; Krakowiak, K. E. *Coord. Chem. Rev.* **1998**, *174*, 179−189.
(2) Doyle, D. A.; Cabral, J. M.; Pfuetzner, R. A.; Kuo, A.; Gulbis, J. M.; Cohen, S. L.; Chait, B. T.; MacKinnon, R. *Science* **1998**, *280*, 69−77.
(3) Gokel, G. W. *Chem. Commun.* **2000**, 1−9. de Mendoza, J.; Cuevas F.; Prados, P.; Meadows, E. S.; Gokel, G. W. *Angew. Chem., Int. Ed.* **1998**, *37*, 1534−1537. Tanake, Y.; Kobuke, Y.; Sokabe, M. *Angew. Chem., Int. Ed. Engl.* **1995**, *34*, 693−694.
(4) For general reviews on calixarenes, see: (a) Gutsche, C. D. *Calixarenes*; The Royal Society of Chemistry: Cambridge, UK, 1989. (b) Böhmer, V. *Angew. Chem., Int. Ed. Engl.* **1995**, *34*, 713−745.
(5) Iwamoto, K.; Shinkai, S. *J. Org. Chem.* **1992**, *116*, 3102−3110.
(6) Cadogan, A.; Diamond, D.; Cremin, S.; McKervey, M. A.; Harris, S. J. *Anal. Proc.* **1991**, *28*, 13−14.
(7) Chan, W. H.; Lee, A. W. M.; Kwong, D. W. J.; Tam, W. L.; Wang, K.-M. *Analyst* **1996**, *121*, 531−534.
(8) Nijenhuis, W. F.; Buitenhuis, E. G.; de Jong, F.; Südholter, E. J. R.; Reinhoudt, D. N. *J. Am. Chem. Soc.* **1991**, *113*, 7963−7968.
(9) Dijkstra, P. J.; Bunink, J. A. J.; Bugge, K.-E.; Reinhoudt, D. N.; Harkema, S.; Ungaro, R.; Ugozzoli, F.; Ghidini, E. *J. Am. Chem. Soc.* **1989**, *111*, 7567−7575.
(10) Ghidini, E.; Uggozoli, F.; Ungaro, R.; Harkema, S.; El-Fadl, A. A.; Reinhoudt, D. N. *J. Am. Chem. Soc.* **1990**, *112*, 6979−6985.
(11) Casnati, A.; Pochini, A.; Ungaro, R.; Bocchi, C.; Ugozzoli, F.; Egberink, R. J. M.; Struijk, H.; Lugtenberg, R.; de Jong, F.; Reinhoudt, D. N. *Chem. Eur. J.* **1996**, *2*, 436−445.
(12) Part of this work has been published as a preliminary communication: Schmitt, P.; Beer, P. D.; Drew, M. G. B.; Sheen, P. D. *Angew. Chem., Int. Ed. Engl.* **1997**, *36*, 1840−1842.

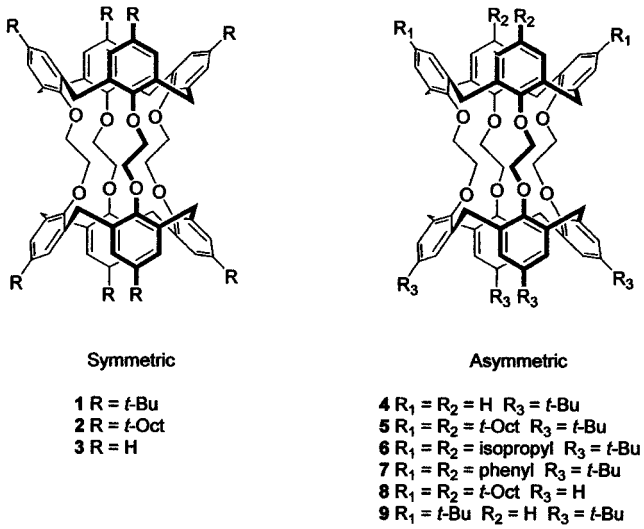

Figure 1. Calix[4]tubes.

oxygen donor atoms for metal complexation (Figure 1). Inclusion of the calix[4]arene units imparts a size discriminatory filter for entry of cations in a manner similar to the tyrosine-based filter[1,13] of a cellular potassium ion channel.

To test the hypothesis that upper rim functionality would play an important role in the potassium complexation properties of calix[4]tubes, a number of tubes with different para substituents were synthesized. Initially, *p-tert*-butylcalix[4]arene[14] was replaced by calix[4]arene[15] or 1,3-*p-tert*-butylcalix[4]arene[16] to determine the influence of the extent of para substitution on complexation. Subsequently, *tert*-octyl,[17] isopropyl,[18] and phenyl[19] groups were studied, allowing investigation of the effects on potassium uptake of increased solubility and steric bulk, nontertiary substitution, and increased π-cation interactions.

The synthesis of the symmetric calix[4]tube **1** was achieved in 51% yield via the reaction of *p-tert*-butylcalix[4]arene with *p-tert*-butylcalix[4]arene tetratosylate in the presence of K_2CO_3 in acetonitrile. These conditions proved unsuitable for the preparation of asymmetric calix[4]tubes in sufficient yield or purity. However, alteration of the solvent for tube formation to the higher boiling xylene in the presence of K_2CO_3 enabled isolation of all the calix[4]tubes **2**−**9**. This reaction in which a macropolycyclic cavity is formed in one step proceeds in excellent yield (50−60%) and is templated by the potassium cation only. Similar cyclizations using sodium or cesium carbonate failed to yield any calix[4]tube. All calix[4]tubes were fully characterized and assigned using a combination of NMR (^{1}H, ^{13}C, 2D (gHMBC, gHSQC)), mass spectrometry (MALDI and FAB), and microanalysis.

A standard synthetic scheme is shown (Scheme 1), where for the synthesis of asymmetric tubes two routes can be followed. The known tetraacetate of *p-tert*-octylcalix[4]arene[17] **10** is efficiently reduced to the alcohol **11** on treatment with $LiAlH_4$ and converted to the tetratosylate **12** with *p*-toluenesulfonate in the presence of triethylamine. Interestingly, the yield obtained in the high-temperature tube-forming step varied considerably and could be greatly enhanced by choice of reagents (Table 1). Thus, tube **8** was isolated in only 20% yield from route 1, but can be obtained in 61% yield by treating *p-tert*-octylcalix[4]arene tetratosylate with calix[4]arene (route 2). This variation is based on the relative solubilities of the two reagents in xylene at room temperature and directed us to the preferential use of *p-tert*-butylcalix[4]arene tetratosylate in the synthesis of the asymmetric tubes.

Table 1. Percentage Yield in Calix[4]tube-Forming Step

tube	tetratosylate *p-tert*-butylcalix[4]arene	tetratosylate *p-tert*-octylcalix[4]arene	tetratosylate calix[4]arene
4	66%		10%
8		61%	20%

Structural Determination: Crystal Structures of Calix[4]tubes and K^+ Complex

The structure of **1** contains a crystallographic center of symmetry with the two calix[4]arene units in the well-known flattened, C_2-symmetrical cone conformation (Figure 2). Within the same calixarene macrocycle, each phenyl ring intersects the plane of the four methylene carbon atoms at angles of 89.6(2), 41.3(2), 87.3(2), and 43.7(2)°, respectively, so that alternate rings can be described as vertical and half-vertical. The four ethylene linkages between the calix[4]arenes alternate in two different conformations. Two opposite angles present a trans-like conformation with O−C−C−O torsion angles of ±161.2(6)°, while the remaining two display a gauche-type conformation with O−C−C−O torsion angles of ±47.8(8)°, so that the conformation can be described as tg$\bar{t}$g (t = trans, g = gauche). These gauche torsion angles are associated with the two vertical phenyl rings. In this particular conformation, the central cage composed of eight oxygen atoms cannot form an inclusion complex because of the two trans arrangements.

The structure of **2** also contains a crystallographic center of symmetry[20] (Figure 3). However, two linkages are disordered, with each CH_2 group occupying two different sites with 50% occupancy. The most likely scenario is that individual molecules contain torsion angles of −154.9 and 161.6 or 154.9 and −161.6°. There are no signs of disorder in the other two linkages, which have torsion angles of ±0.5°. These values are unexpectedly small, and because such angles are not observed in our conformational analysis, it seems likely that they are an artifact of the disorder, although the carbon atoms involved showed no signs of unexpected anisotropy. One *tert*-octyl group is also disordered. The four phenyl rings intersect the plane of the four methylene atoms at angles of 83.3(2), 37.4(2), 88.9(2), and 31.2(2)°, with the vertical phenyl rings associated with the gauche O−CH_2−CH_2−O torsion angles as in **1**.

The structure of **1**·K^+ has also been determined and contains an approximate though noncrystallographic C_4 element of symmetry along the main axis of the molecule (Figure 4). All

(13) Dougherty, D. A. *Science* **1996**, *271*, 163−168.
(14) Gutsche, C. D.; Iqbal, M. *Org. Synth.* **1990**, *68*, 234−237.
(15) Gutsche, C. D.; Levine, J. A. *J. Am. Chem. Soc.* **1982**, *104*, 2652−2653.
(16) Dalbavie, J. O.; Regnouf-De-Vains, J. B.; Lamartine, R.; Lecocq, S.; Perrin, M. *Eur. J. Inorg. Chem.* **2000**, *4*, 683−691.
(17) Ohto, K.; Yano, M.; Inoue, K.; Yamamoto, T.; Goto, M.; Nakashio, F.; Shinkai, S.; Nagasaki, T. *Anal. Sci.* **1995**, *11*, 893−902.
(18) Zheng, Y. S.; Huang, Z. T. *Synth. Commun.* **1997**, *27*, 1237−1245.
(19) Juneja, R. K.; Robinson, K. D.; Johnson, C. P.; Atwood, J. L. *J. Am. Chem. Soc.* **1993**, *115*, 3818−3819.

(20) Crystallographic data (excluding crystallographic structural factors) for the structures reported in this paper have been deposited with the Cambridge Crystallographic Data Centre as supplementary publication no. CCDC-100240. Copies of the data can be obtained free of charge on application to The Director, CCDC, 12 Union Road, Cambridge CB2 1EZ, UK. (Fax: int. code +1223 336-033. E-mail: deposit@chemcrys.cam.ac.uk.)

Scheme 1. Synthesis of Calix[4]tube **8**

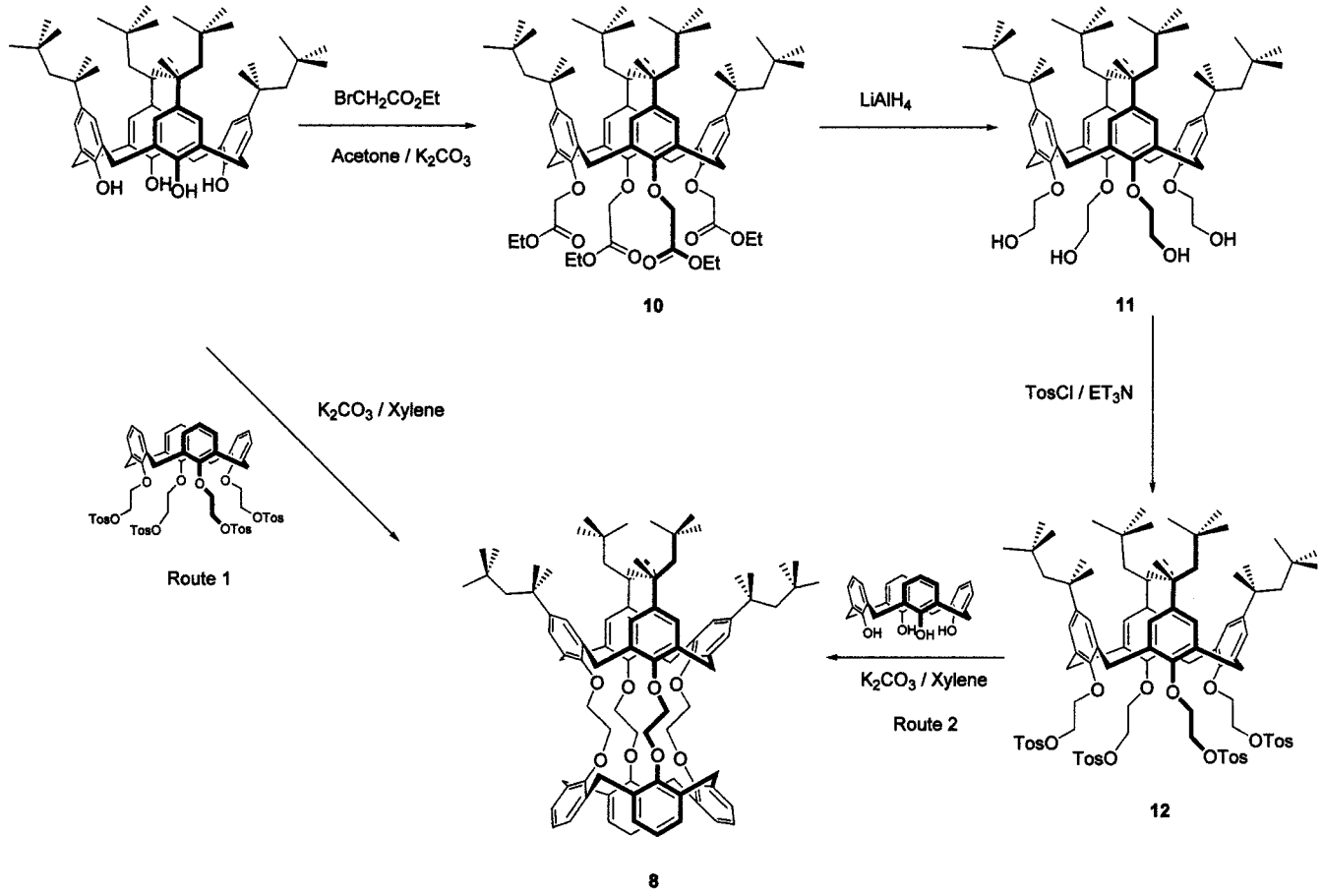

ethylene linkages present a gauche conformation, with the four O−C−C−O torsion angles taking up values of 68.2, 59.8, 52.3, and 61.9° so that the conformation of the structure can be described as gggg. The angles of intersection of the phenyl rings with the mean plane of the four methylene carbon atoms are very similar varying between 64.6(2) and 67.9(2)°.

The potassium ion is located at the center of a slightly flattened cube of the eight oxygen atoms with the K−O distances ranging from 2.759(6) to 2.809(6) Å. The iodide anions are present in the lattice but show no close interactions with the K^+ cations; indeed, the closest contacts are 6.46 and 7.40 Å. There are two methanol molecules in the cone cavities. Such solvent inclusion is a feature of many structures of calix[4]arene in the cone conformation, although with the C_2 distorted flattened cone, as for example in **1**, solvent entry is not possible because of the close proximity of the two vertical phenyl rings.

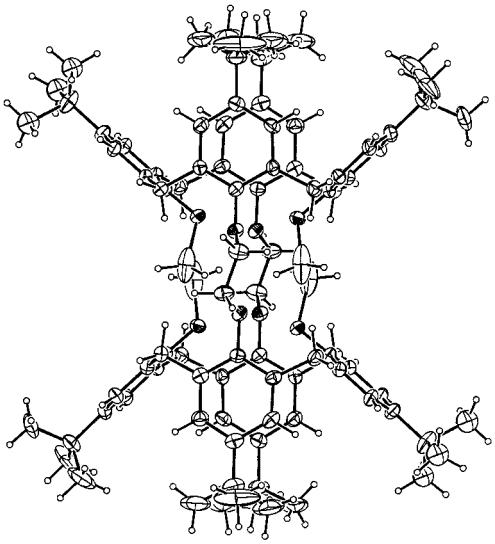

Figure 2. Crystal structure of the centrosymmetric calix[4]tube **1** in **1**·$2.5C_6H_6$, with ellipsoids at 20% probability. Hydrogen atoms are included with small arbitrary radii. The benzene solvent molecules are not shown.

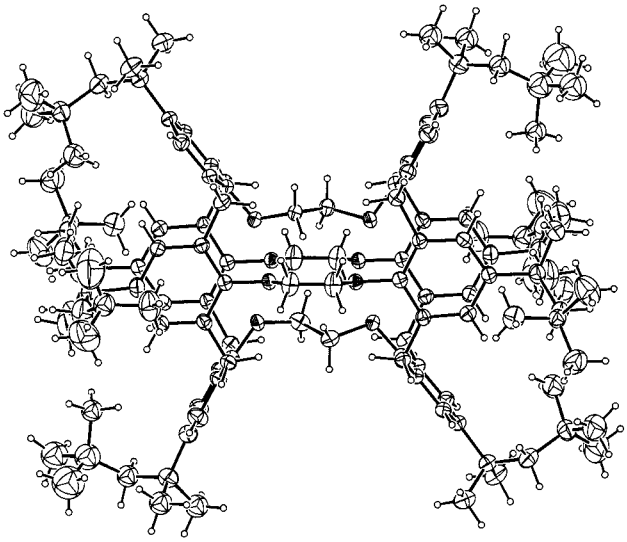

Figure 3. Plot of the crystal structure of R = *tert*-octyl. Ellipsoids shown at 20% occupancy. One unique set of positions of the disordered *tert*-octyl group is shown.

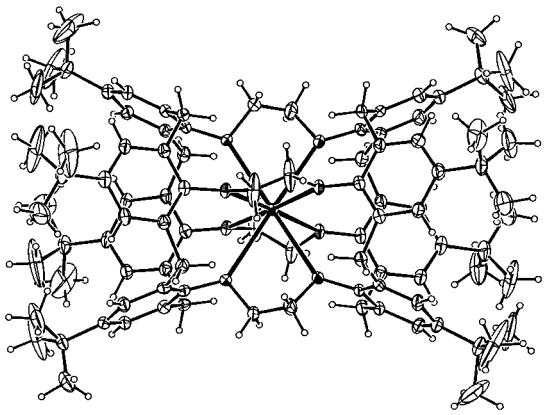

Figure 4. Structure of the K^+ complex of calix[4]tube **1** in crystals of **1**·1.3$CHCl_3$·4CH_3OH·H_2O. A potassium ion is located at the center of 1, and two methanol molecules in the cone cavities. Ellipsoids are drawn at 20% probability. Hydrogen atoms are included with small arbitrary radii. The chloroform and water molecules are not shown.

Structural Determination in Solution: NMR

The unexpected C_i symmetry found in the solid state for the uncomplexed tube, with each calix[4]arene unit adopting a flattened cone conformation, is also maintained in solution. The ^{1}H NMR of compound **8** (Figure 5a) is representative of all the tubes synthesized. A doubling of the peaks is observed for every residue, excluding the methylene bridge, confirming the presence of two inequivalent aryl residues within each calix[4]arene. This same complexity is also seen in the ^{13}C NMR spectra of the tubes. Although the spectral characteristics are retained up to a temperature of 50 °C without broadening, saturation transfer experiments show that exchange of the two flattened cone conformers is possible in chloroform on the NMR time scale. k_{exch} at 328 K, calculated by EXSY experiments, varied over a large range, e.g., 0.94 s^{-1} for **1** and 2.95 s^{-1} for **2**. [Note: Slow exchange rates were determined from 1D-EXSY ($\pi/2-t_1-\pi/2-t_m-\pi/2-$obs) experiments. Rate constants were calculated from the program CIFIT[35] with T1 relaxation rates estimated from inversion recovery experiments.]

Calix[4]tube **9**, in which one of the calix[4]arene units is 1,3-functionalized, exhibits more complex spectra in accordance with the presence of two conformational isomers (Figure 6). Saturation transfer experiments show the isomers to be in exchange at room temperature in chloroform. The more favored isomer (1.6:1) has been identified by NOE experiments to be conformer A, in which minimal steric interactions occur between the two *p-tert*-butyl residues.

Complexation of Potassium

Initial qualitative experiments demonstrated that on complexation with an excess of potassium iodide in chloroform/methanol (4:1) new signals due to a calix[4] tube−cation complex can be observed (Figure 5b). In this case, the spectra simplify to give single peaks for all residues confirming that, once the cation is complexed, the tube adopts a time-averaged C_4 structure in which all aryl residues are equivalent, as observed in the solid state. The downfield shift of all calix[4]arene protons on complexation (between 0.22 and 0.92 ppm) in combination with the upfield shift within the ethylene unit (0.23 ppm) is consistent with a displacement of the electron density to the equatorial plane due to the complexed positively charged cation.

As the rate of complexation and decomplexation of potassium by calix[4]tubes **1**−**9** proved slow on the NMR time scale, uptake could be measured by direct integration of peaks for complexed and uncomplexed species. Thus, a series of quantitative complexation experiments were undertaken in which a 1 mM solution (0.5 mL) of a calix[4]tube in chloroform/methanol (4:1) was added to 20 equiv (10 μmol) of solid potassium iodide and a NMR spectrum was recorded at 5 min intervals for 2 h. Such heterogeneous complexation methods are dictated by the low solubility of calix[4]tubes in non-halogenated solvents and the marked effect of counterion on complexation (vide infra). Analysis of the data gave the complexation profiles shown in

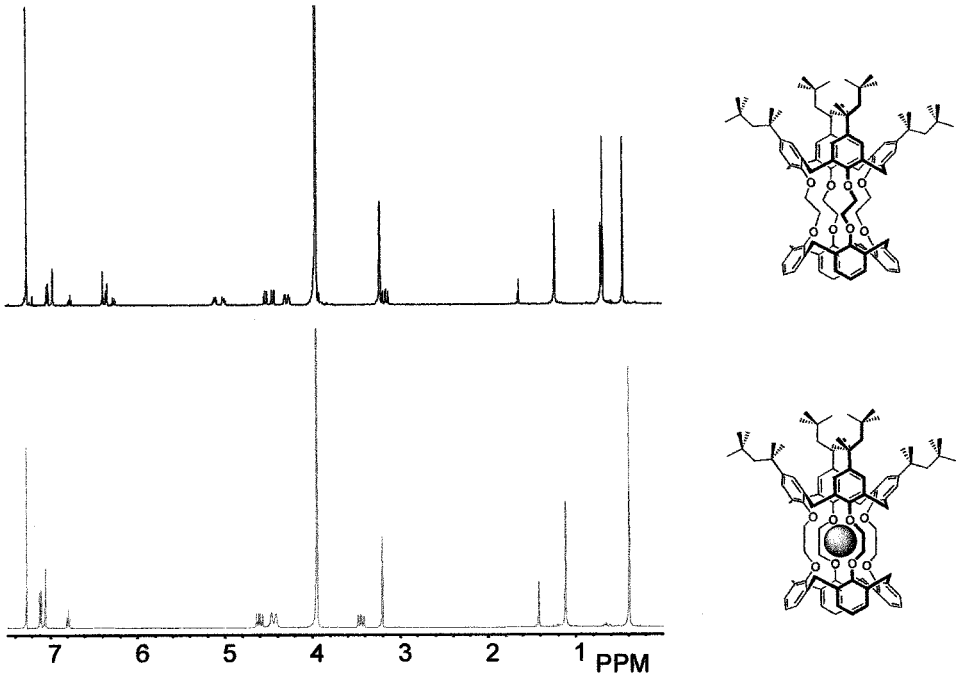

Figure 5. ^{1}H NMR of **8** in chloroform/methanol (4:1): (a) absence of K^+; (b) after 4 days in the presence of 20 equiv of KI.

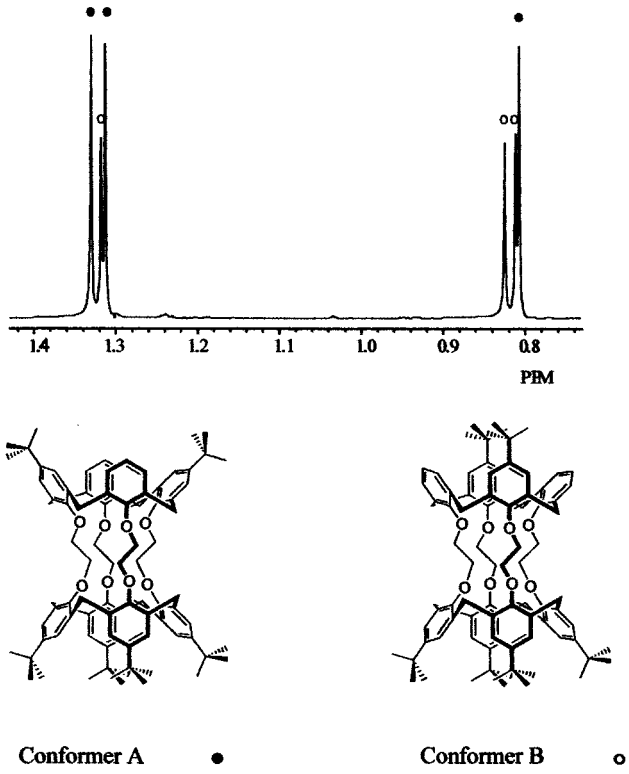

Figure 6. A typical region from the NMR of calix[4]tube **9**, showing the relative distribution of conformers A and B.

Figure 7. Three types of calix[4]tubes can be categorized: those with fast and expected exponential uptake, those with intermediate kinetics, often showing sigmoidal complexation curves, and those with slow complexation kinetics.

Figure 7a shows that calix[4]tube **1** is most efficient at complexing potassium, achieving equilibrium within 2 h with $k_{obs} = 3.9 \times 10^{-2}$ s^{-1} and having a half-life of 25 min. Surprisingly, removal of only two *p*-*tert*-butyl moieties **9** has a dramatic effect on potassium uptake, with only 50% complex formation at 2 h ($k_{obs} = 6.8 \times 10^{-3}$ s^{-1}). Similarly, a further drop in complexation rate is seen for tube **4**, where effectively all four *p*-*tert*-butyl moieties of one calix[4]arene unit have been removed (Figure 7b). Here, only 10% of the calix[4]tube is present as the complexed species after 2 h, although full conversion is achieved within 2 days. Further elaboration to give the *p*-H calix[4]tube reduces the rate considerably: over 15 h, only 11% of the complexed species is observed.

Interestingly, the introduction of *p*-*tert*-octyl substituents to increase solubility had an unexpected effect on the rate of complexation. For both **2** and **5**, slightly sigmoidal curves are obtained in the 2 h observation period; initial slow uptake is followed by a more rapid complexation after 1 h (Figure 7a). This profile suggests that complexation does not follow the simple pseudo-first-order kinetics expected from the reaction conditions and precludes measurement of k_{obs}. Surprisingly, replacement of one *p*-*tert*-butylcalix[4]arene unit with *p*-*tert*-octylcalix[4]arene **5** or replacement of both units **2** has a similar effect on the rate of complexation; both receptors have a $t_{1/2}$ of around 2 h.

Introduction of both isopropyl- and phenylcalix[4]arene units has a detrimental effect on potassium binding. Of particular interest are the results for **7**: inclusion of phenyl units could

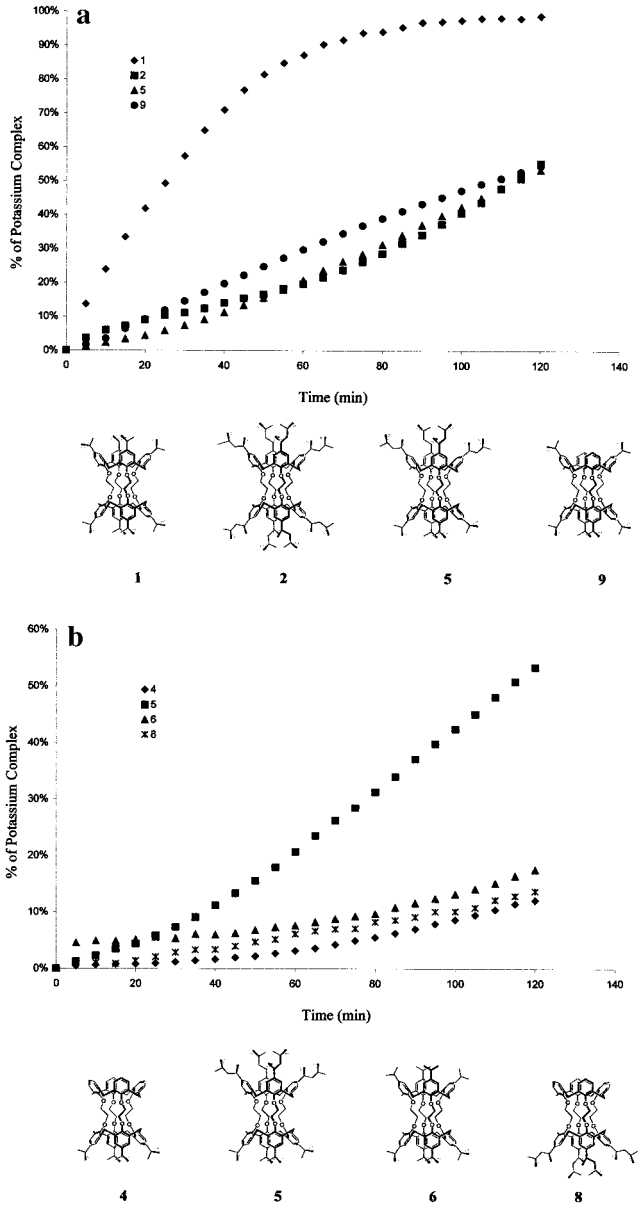

Figure 7. (a) Uptake of K^+ by calix[4]tubes **1**, **2**, **5**, and **9** from 20 equiv of KI in chloroform/methanol (4:1) at ambient temperature calculated from NMR integration of complexed and uncomplexed species at 5 min intervals. (b) Uptake of K^+ by calix[4]tubes **4**, **5**, **6**, and **8** from 20 equiv of KI in chloroform/methanol (4:1) at ambient temperature calculated from NMR integration of complexed and uncomplexed species at 5 min intervals.

be postulated to increase the effectiveness of π-cation interactions and thus increase uptake of potassium if entry of the cation occurs through the calix[4]arene filter. However, not only is the complexation rate slow, but full complexation is not achieved and an equilibrium of only 70% is reached after 4 days. Analysis of the crystal structure for *p*-phenylcalix[4]arene[18] suggests that the phenyl moiety is skewed with respect to the calixarene core and thus may effectively sterically inhibit *axial* cation entry to the calixarene unit.

In an attempt to rationalize the large rate variation of potassium cation binding by the range of symmetric and asymmetric calix[4]tubes for complexation to proceed via the axial route, passing through the calix[4]arene annulus, a two-step complexation pathway may be envisaged. In the first step, the potassium cation interacts with the arene units through

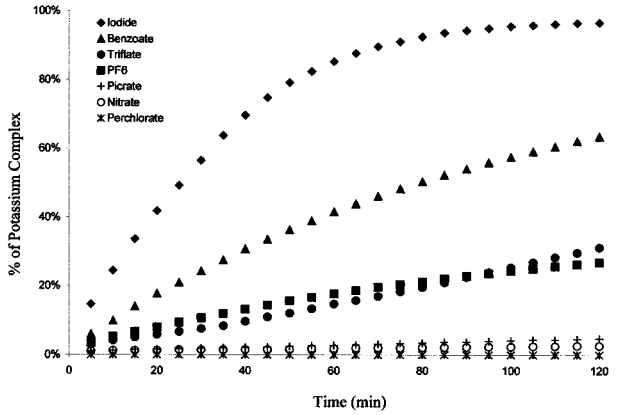

Figure 8. Uptake of K^+ by calix[4]tube **1** for a range of potassium salts.

π-cation interactions. This is followed by a subsequent step where the metal cation is complexed in the eight oxygen donor cage, the rearrangement of which is evidenced by spectral changes. It could be postulated that increasing the strength of π-cation interactions, as in the case of both phenyl and *p-tert*-octylcalix[4]arenes, stabilizes the intermediate, in which the K^+ ion is retained within the calix[4]arene bowl[21] and thus reduces the rate of entry of the cation into the binding site formed by the oxygen array and the concomitant spectral change. However, it is unlikely that such a large range in rate could be accounted for by this hypothesis. If data from the crystal structures and modeling studies are considered, a second hypothesis can be made: the rate-limiting step is a conformational polyether cage rearrangement of the cation binding site, the initial torsion angles and orientations of which and subsequent ease of conformational mobility are dictated by the substituents at the upper rim (vide supra).

Effect of Counteranion on Complexation

Complexation of **1** with a range of potassium salts was also undertaken to investigate the effect of counteranion on binding of the cation. Surprisingly, large variations in uptake were observed (Figure 8): complexation was most effective with an iodide counterion but was also efficient with hexafluorophosphate, benzoate, and triflate. However, minimal or no uptake is achieved with nitrate, perchlorate, and picrate. In these solid−liquid extraction investigations, a correlation between the rate of potassium cation uptake and the respective KX lattice energy, calculated from the Kapustinskii equation on the basis of relative thermochemical anion radii,[22] may be predicted. Although this postulate can account for the relative rates of KI > KNO_3 ($rI^- = 0.210 > rNO_3^- = 0.196$), it fails for the remaining potassium salts.

Competition with 2.2.2.Cryptand

To assess the strength of binding of the potassium cation within the tubular cage, a competition experiment with the known potassium-selective 2.2.2.cryptand[23] was undertaken. Calix[4]tube **1** was precomplexed with potassium (as the iodide) in chloroform/methanol (4:1) for 24 h and then filtered, and the solution was added to a 20-fold excess of 2.2.2.cryptand. Observation of the NMR spectrum over fixed time intervals showed the calix[4]tube complex to be highly stable with only 28% conversion to the uncomplexed species (through complexation with the competing cryptand) after 15 h.

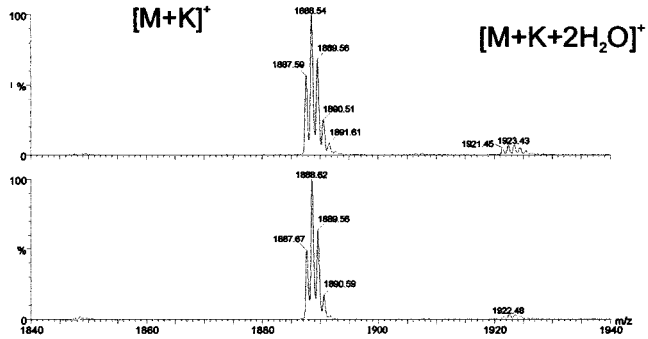

Figure 9. Electrospray mass spectra: (a) calix[4]tube **2** + 10 μmol of all alkali metal iodides; (b) calix[4]tube **2** + 2.5 μmol of KI, 10 μmol of LiI, NaI, RbI, CsI.

Selectivity of Potassium Cation Complexation

The strong binding of potassium cation prompted us to evaluate uptake of other group 1 metal cations. Complexation of barium, a similarly sized doubly charged cation, was also investigated. NMR spectra were recorded after a 48 h pretreatment of 1 mM solutions of tubes **1**−**9** in chloroform/methanol (4:1) with a 20-fold excess of either Na^+, Rb^+, K^+, Cs^+, or Ba^{2+} as the metal iodides. Tubes **3**−**9** showed no uptake of any cation apart from potassium. Less than 5% Rb^+ was taken up by tube **1**, whereas after 48 h tube **2** showed 10% uptake of Na^+ (100% of potassium is complexed by both receptors at this time point). Thus, these hosts can be considered to be highly selective for potassium over all the group 1 metals and barium, in great contrast to calix[4]crown-based systems, which despite having high Na^+/K^+ selectivity show significant uptake of rubidium.[7−10]

Competitive complexation studies were undertaken using electrospray mass spectrometry techniques. This method has recently attracted much interest for the evaluation of host−guest complexation and ion selectivity with calixcrown systems.[24−26] These studies have shown that the ions seen in the gas phase accurately reflect the composition of host−guest complexes in solution. Initially, Calix[4]tubes **1**, **2**, **5**, and **9** were pretreated with a mixture of alkali metal iodides in chloroform/methanol (4:1) to give a host:guest ratio of 1:20 (10 μmol of each cation). In all spectra (e.g., Figure 9), peaks were observed only for [M + K^+] and [M + K^+ + $2H_2O$]. Further analysis using a dilution approach, in which the concentration of potassium alone was reduced to 2.5 μmol while the competing cation concentrations were maintained at 10 μmol, once again gave only the potassium species, demonstrating the remarkable high selectivity for potassium of all calix[4]tubes.

Molecular Modeling

Molecular modeling was undertaken to ascertain the mode of entry of potassium into the calix[4]tube. Two routes can be

(21) Lhotak, P.; Shinkai, S. *J. Phys. Org. Chem.* **1997**, *10*, 273−285.
(22) Moyer, B. A.; Bonnesen P. V. In *Supramolecular Chemistry of Anions*; Bianchi, A., Bowman-James, K., Garciá-España, E., Eds.; Wiley-VCH: New York, 1997; pp 1−41.
(23) (a) Dietrich, B.; Lehn, J. M.; Sauvage, J. P. *Tetrahedron Lett.* **1969**, 2885−2888. (b) Dietrich, B.; Lehn, J. M.; Sauvage, J. P. *Tetrahedron Lett.* **1969**, 2889−2892.
(24) Allain, F.; Virelizer, H.; Moulin, C.; Jankowski, C. K.; Dozol, J. F.; Tabet, J. C. *Spectroscopy* **2000**, *14*, 127−139.
(25) Blanda, M. T.; Farmer, D. B.; Brodbelt, J. S.; Goolsby, B. J. *J. Am. Chem. Soc.* **2000**, *122*, 1486−1491.
(26) Goolsby, B. J.; Brodbelt, J. S.; Adou, E.; Blanda, M. T. *Int. J. Mass Spectrom.* **1999**, *193*, 197−204.

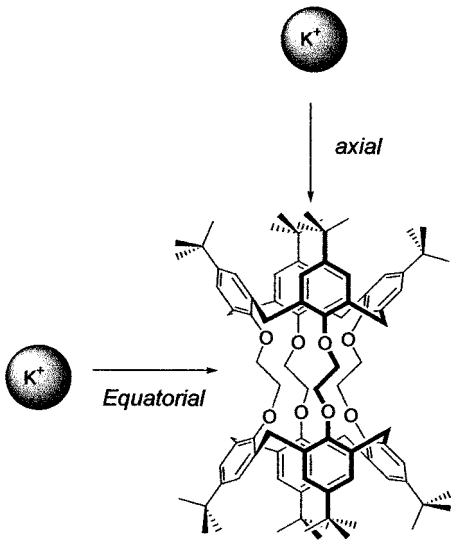

Figure 10. Potential routes for complexation of potassium by calix[4]tubes.

identified (Figure 10): the *axial* route, where the cation initially passes through the calix[4]arene filter and then onto the polyether binding site, and the *equatorial* route, in which the cation is complexed directly by rearrangement of the cryptand-like binding site. The NMR kinetic results showing dramatic variation in the rate of potassium complexation on alteration of the calix[4]arene upper rim substituent tend to suggest the axial route of complexation, as NMR structural investigations show the polyether binding region to be conserved.

A molecular dynamics run in the gas phase was carried out at 300 K on **1** using Cerius2[27] together with the Universal force field.[28] Atomic charges were calculated using the Gasteiger method implemented in Cerius2. The atoms in the $O-CH_2-CH_2-O$ links were given charges taken from ref 29, and the charges on the rest of the molecule were then adjusted to give a neutral tube. The starting model was taken from the crystal structure of **1**. The step size was 1.0 fs, and the simulation was carried out for 500 ps. The variations in the O−C−C−O torsion angles are shown in Figure 11. Each torsion angle remains either trans or gauche (Figure 11), thus maintaining the *tgtg* conformation, but changes in sign are occasionally observed. [Note: Generic (i.e., signless) conformations are given in italics.]

In order, inter alia, to investigate this observation, we also carried out a conformational analysis on the free ligand using molecular dynamics. The crystal structure of **1** was minimized via molecular mechanics to create the starting model. The structure was heated to 3000 K with a step size of 1 fs. One thousand structures were saved at 100 fs intervals and subsequently energy minimized with molecular mechanics using the Universal force field. The resulting unique structures are shown in Table 2, together with the final energies. It should be borne in mind that the arrangement of the *tert*-butyl groups is also variable and, therefore, that conformations with similar O−C−C−O bridge torsion angles may have slightly different energies. For that reason, the conformational analysis was repeated with a calix[4]tube in which the *tert*-butyl groups were replaced by hydrogen atoms. The lowest energy conformation for each set

(27) Cerius2 v3.5, Molecular Simulations Inc., San Diego, CA, 1999.
(28) Rappe, A. K.; Casewit, C. J.; Colwell, K. S.; Goddard, W. A., III; Skiff, W. M. *J. Am. Chem. Soc.* **1992**, *114*, 10024−10035.
(29) Varnek, A.; Wipff, G. *J. Comput. Chem.* **1996**, *17*, 1520−1531.

Table 2. Low-Energy Conformations for Calix[4]tube **1**

	energies (kcal mol^{-1})					
conformation	R = *tert*-butyl	R = H	O–C–C–O torsion angles (°) for R = *tert*-butyl			
tgtg	372.40	313.51	139.4	47.4	165.0	46.6
$tg\bar{t}\bar{t}g$	373.59	315.08	171.4	−44.8	−127.9	−45.0
$tgt\bar{g}$	374.11	315.74	174.6	43.8	129.1	−36.8
$tg\bar{t}g$	374.48	314.92	150.3	43.0	−150.3	−43.0
$t\bar{g}t\bar{g}$	376.14	317.06	171.4	−42.0	128.4	−38.0
ttgg	381.10	325.89	175.2	177.1	64.8	64.1
$ttt\bar{g}$	381.37	320.02	176.4	176.4	173.2	−74.9
$ttg\bar{g}$	383.11	327.16	175.4	172.9	62.4	−67.1
$t\bar{t}gg$	383.90	324.73	161.1	−157.7	103.0	47.2
$t\bar{g}\bar{g}\bar{g}$	386.52	331.54	171.8	−72.4	−68.3	−70.0
$tgg\bar{g}$	387.62	330.75	175.5	67.0	67.3	−70.7
$tg\bar{g}g$	389.59	333.86	173.8	70.5	−69.1	71.7
$g\bar{g}gg$	396.95	338.91	69.7	−74.8	70.6	71.3
$gg\bar{g}\bar{g}$	396.99	343.80	70.8	71.4	−70.2	−70.6

of O−C−C−O bridge torsion angles is included in the table. The five lowest energy conformations are all of the *tgtg* type, although exhibiting variations in sign, viz. tgtg at 372.40 kcal mol^{-1}, $tg\bar{t}\bar{t}g$ at 373.59 kcal mol^{-1}, $tgt\bar{g}$ at 374.11 kcal mol^{-1}, $tg\bar{t}\bar{t}g$ at 374.48 kcal mol^{-1}, and $t\bar{g}t\bar{g}$ kcal mol^{-1} at 376.14 kcal mol^{-1}, respectively. Then come two *tttg* and *ttgg* type conformations, with energies in the range 381.10−384.68 kcal mol^{-1}, and *tggg* conformations (386.52−389.59 kcal mol^{-1}). The final set of conformations are the all-gauche, with energies of 396.96−396.99 kcal mol^{-1}. The results for the cage R = H are similar and show that the presence of *tert*-butyl groups does not have a significant effect on the conformational analysis. It is interesting that in this conformational analysis the *gggg* conformation necessary for metal complexation in the cavity is one of the highest energies. This result is also apparent in the MD simulation of the ligand at 300 K, where the *tgtg* conformation is observed throughout, although there is a change in the sign of the torsion angles.

We then repeated the molecular dynamics simulation for the cages with R = H and R = *tert*-octyl. The starting model for R = H was taken from the crystal structure of **1** with the *tert*-butyl groups replaced by a hydrogen atom and for R = *tert*-octyl from the crystal structure of **2**. Variations in torsion angles with time are significantly different from the trace shown in Figure 11 for R = *tert*-butyl in that, while both maintain the *tgtg* conformation, there is much less frequent change in the sign of the torsion angles. It seems likely that the lack of change in torsion angle for R = H and R = *tert*-octyl has different explanations. Thus, for the R = *tert*-octyl structure, the bulky *tert*-octyl groups interlock in the $ggg\bar{g}$ conformation and thus prevent any change in conformation. For the R = H structure, it would appear that the lack of alkyl groups at the top of the phenyl rings deprives the cage of any impetus for changing its conformation. Thus, it can be concluded that with the R = *tert*-butyl structure the *tert*-butyl groups play an important role in the change of conformation. These results are consistent with the data provided in this paper showing the variation in potassium complexation properties with R groups.

As the structure of $\mathbf{1}\cdot K^+$ has also been determined, we then wished to consider how the conformational change from $tg\bar{t}\bar{t}g$ in the free ligand to gggg occurs in the formation of the potassium complex. This was first investigated via molecular

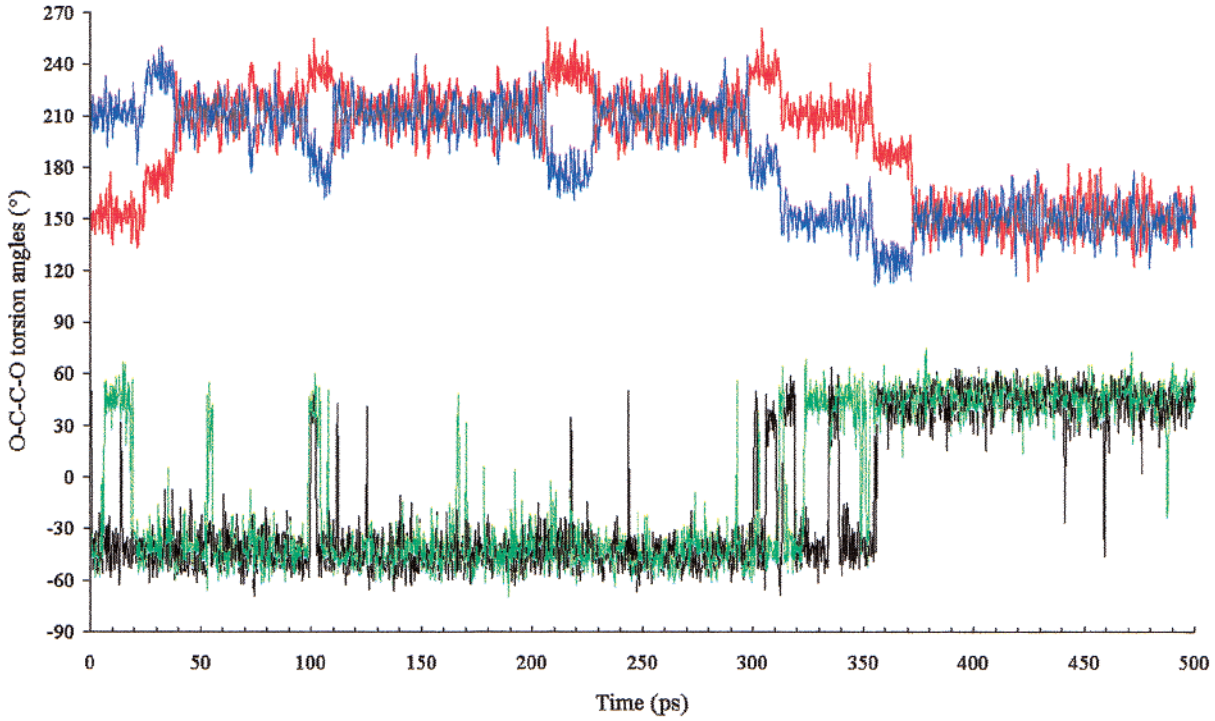

Figure 11. Plot of the four O−C−C−O torsion angles during the 500 ps simulation. for R = *tert*-butyl. The red and blue curves represent torsion angles from the 1,3-linkages (with O−CH_2−CH_2−O torsion angles trans) and green and black from the 2,4-linkages (with O−CH_2−CH_2−O torsion angles cis).

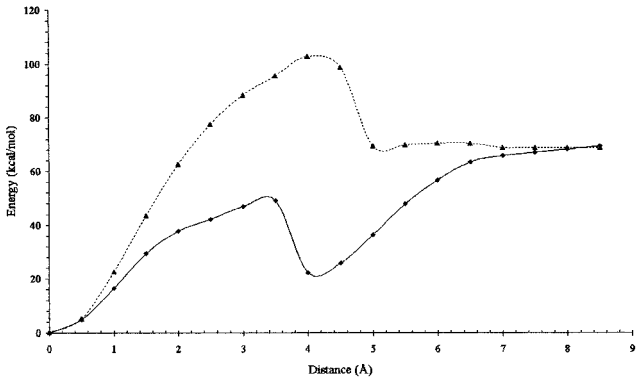

Figure 12. Results of molecular mechanics simulation showing energy (kcal mol^{-1}) against the position of the K^+ cation from the center of the tube (Å).

mechanics calculations. The obvious pathway for the cation was via the principal axis of the calixarene, but a pathway perpendicular to the principal axis was also considered. The potassium ion was positioned at different distances (in 0.5 Å intervals) either along the principal axis or perpendicular to it. At each placement, molecular mechanics energy minimization was carried out but with the distance of the metal from the center of the calix tube constrained. The resulting energy curve is shown in Figure 12 and confirms that the lower energy pathway involves the cation entering the calix[4]tube adjacent to the *tert*-butyl groups along the principal axis and proceeding along the axis to the center of the tube. With this axial pathway there is a clear indication of a local energy minimum at an anion-to-tube center distance of ca. 4.0 Å. It is noteworthy that the conformation of this minimized structure containing the cation is tg$\bar{t}$g$\bar{}$, and this could indicate an intermediate stable species. This structure can be compared with several crystal structures in which an alkali metal is similarly placed within a calix[4]-arene. Particularly apposite is the position of cesium in CsI·p-*tert*-butylcalix[4]arene,[30] where the metal interacts with the four phenyl rings. Here the calix[4]arene has crystallographic 4-fold symmetry, and the distance of the metal from the center of the four oxygen atoms at the bottom rim of the cone is 3.57 Å, so that the Cs atom is almost coplanar (within 0.04 Å) with the four atoms at the top of the four phenyl rings. In this structure the angles between the phenyl rings and the plane of the four methylene groups are 57.4°. Two other relevant structures[31] show substituted calix[4]arenes in the 1,3-conformation with one or two potassium ions bonded to four oxygen atoms of two diethylcarbamoylmethoxy substituents but also sandwiched between two phenyl rings.

To investigate this possible reaction path, a molecular dynamics simulation was also carried out on the **1**·K^+ complex using the same methodology as for **1**. The K^+ ion was given a charge of +1, but the charges on atoms in the tube remained unchanged. The starting model included the structure of the free calix[4]tube found in the crystal, with the O−C−C−O linkages in the tg$\bar{t}$g$\bar{}$ conformation and the K^+ ion positioned level with the top of the four phenyl rings of the calix[4]arene. The step size was 1.0 fs, and the dynamics simulation was run for 500 ps at 400 K. (Runs at 300 K did not produce sufficient events in short simulations.) The K^+ cation remained in the cavity close to the top of the four phenyl rings of the calix[4]arene for approximately 152 ps when it moved into the central cavity within 1 ps to become bonded to the eight oxygen atoms. Concomitant with this change in position of the K^+ cation, the two O−C−C−O trans torsion angles changed to gauche. This

(30) Harrowfield, J. M.; Ogden, M. I.; Richmond, W. R.; White, A. H. *J. Chem. Soc., Chem. Commun.* **1991**, 1159−1161.
(31) Beer, P. D.; Drew, M. G. B.; Gale, P. A.; Leeson, P. B.; Ogden, M. I. *J. Chem. Soc., Dalton Trans.* **1994**, 3479−3485.

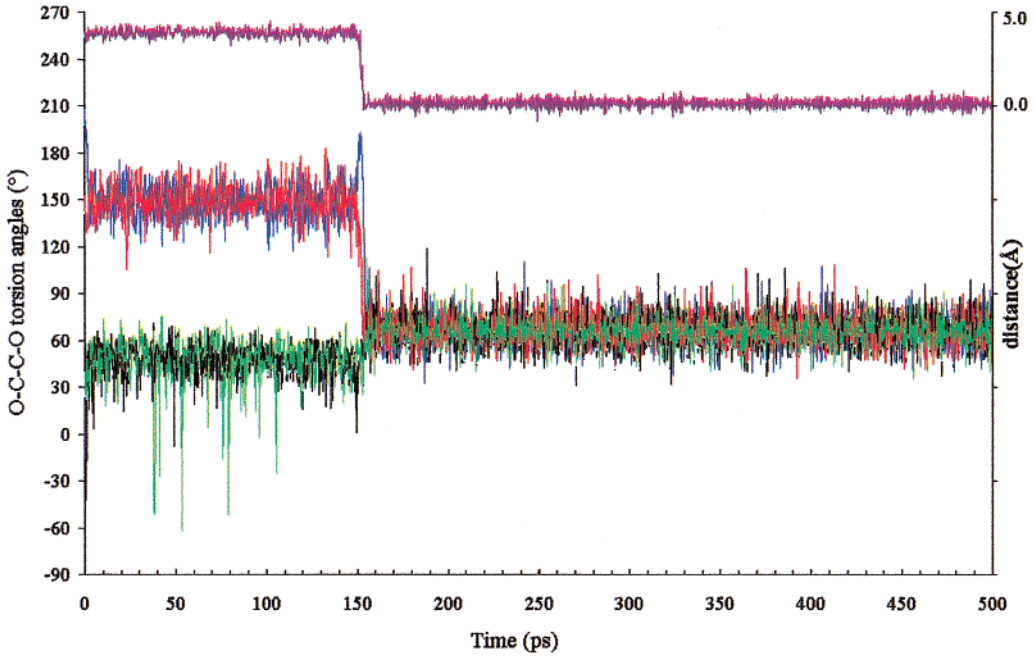

Figure 13. (*y* axis on left) Plot of the four O−C−C−O torsion angles during the 500 ps simulation for **1**·K^+. The red and blue curves represent torsion angles from the 1,3-linkages and green and black from the 2,4-linkages. (*y* axis on right) Plot of the distance (purple) of the K^+ ion from the center of the tube.

Table 3. Four All-Gauche Conformations Located from a Conformational Analysis of **1**·K^+

conformation	energy (kcal mol^{-1})	torsion angles (°)			
gggg	275.88	66.4	65.7	66.3	66.0
ggg$\bar{g}$	278.89	66.7	66.9	67.9	−65.8
gg$\bar{g}\bar{g}$	279.28	66.3	65.9	−66.7	−66.3
g$\bar{g}$g$\bar{g}$	281.55	68.2	−68.0	68.1	−68.3

is shown in Figure 13, a plot of variations of relevant parameters during the simulation, including the four torsion angles and the distance of the K^+ from the center of the cavity. Having proceeded to the center of the cavity, the K^+ cation remained in place throughout the remainder of the simulation, and the four torsion angles remained at $^+$g values equivalent to those found in the crystal structure of **1**·K^+. However, when a conformational analysis was carried out using the same methodology as for **1** described above, it became apparent that there were four distinguishable conformations: gggg, ggg$\bar{g}$, gg$\bar{g}\bar{g}$, and g$\bar{g}$g$\bar{g}$. The energies of these conformations are given in Table 3 and show that the structure found in the crystal, with a 4-fold symmetry, indeed has the lowest energy of the four.

The movement of the K^+ ion to the center of the tube was considered in more detail. In some simulations (not reported here in detail), the K^+ ion moves from the intermediate position close to the phenyl rings out of the tube. However, in most simulations, including the one reported here, the K^+ ion moves to the center of the tube via the *tert*-butyl rim. At the start of the simulation (Figure 13), the tgt$\bar{g}$ conformation is maintained. After the K^+ cation has moved to the center of the tube, all four torsion angles oscillate only between the gauche angles. The K^+ ion oscillates around 4.18 Å from the center of the tube until passing through to the center of the tube.

Figure 14 shows five snapshots within the simulation which illustrate the movement of the potassium from the intermediate position, where it interacts with the phenyl rings, to the central position attached to the eight oxygen atoms. In Figure 14, (a) shows the starting position of the potassium ion, which is maintained for 152.20 ps. During this time, it moves to the top of the tube (b) but does not leave the tube. After 153.50 ps (c), the ion begins to move to the center of the tube. At the same time, first one O−CH_2−CH_2−O torsion angle and then the other changes from trans to gauche until all four angles are gauche and the ion is at the center of the tube (d) after 153.75 ps. The K^+ cation then remains in the center of the tube for the remainder of the 250 ps simulation (e).

The molecular dynamics simulation in conjunction with the previous molecular mechanics calculation shows clearly the series of events that lead to the encapsulation of the potassium ion in the calix[4]tube. The tube has the lowest energy *tgtg* conformation in solution. The potassium ion enters the tube through the top of the calix[4]tube and proceeds to an intermediate position, where it is stabilized by interactions with the phenyl rings. From this position it can either return to a position outside the tube or proceed into the center of the cage, concomitant with a change in the conformation of the tube to *gggg*.

It remains to consider why the tube is so selective for potassium. We calculated the energy profile for the tube with a metal ion in the center using our published method.[32] Here the M−O distances were fixed at specific values, and the remainder of the structure was allowed to converge to the lowest possible energy, thus providing a plot of M−O against energy. The plots for all four possible conformations are shown in Figure 15. As can be clearly seen, the minimum energies are found around 2.84 Å, equivalent to the K−O distances observed in the crystal structure of **1**·K^+.

However, it is possible that selectivity is also controlled in part by the positions of the phenyl rings which can form a switch

(32) Costa, J.; Delgado, R.; Drew, M. G. B.; Felix, V.; Henriques, R. T.; Waerenborgh, J. C. *J. Chem. Soc., Dalton Trans.* **1999**, 3253−3265.

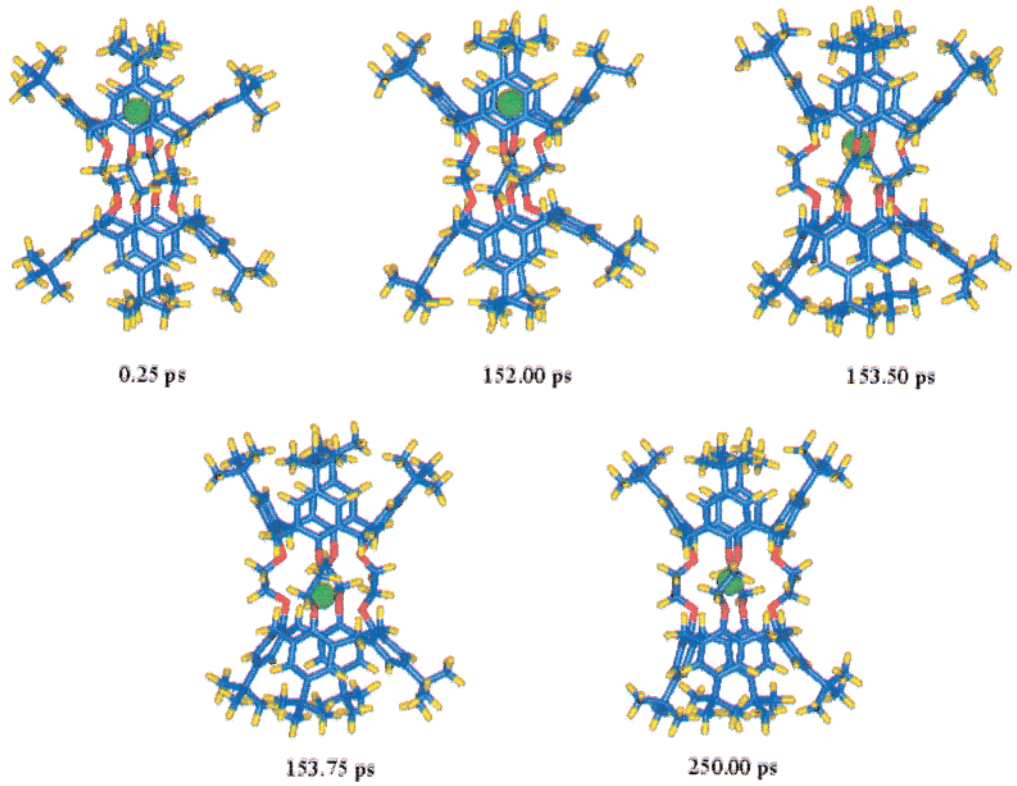

Figure 14. Five snapshots showing the movement of the K^+ ion in the calix[4] tube during the simulation. The snapshots were taken at the beginning of the simulation (a), during the 2 ps (after 152 ps) where the change in structure occurs (b, c, d), and at the end of the simulation (e). Potassium is green, oxygen red, carbon blue, and hydrogen yellow.

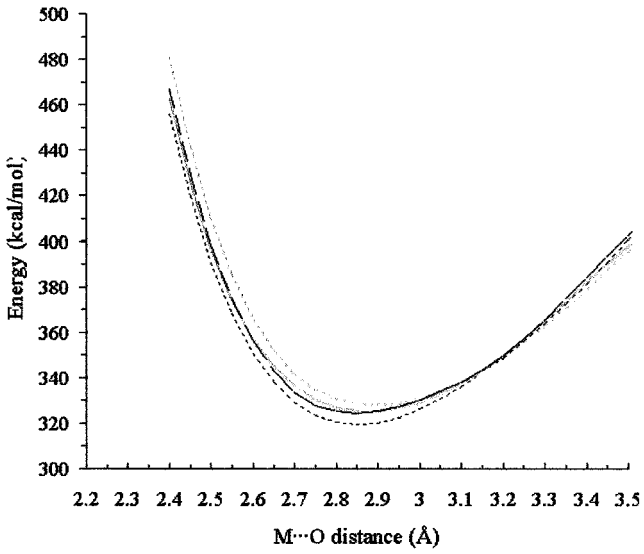

Figure 15. Plot of energy against M−O distance for the **1**·M^+ structure in **1**. Four possible all-gauche conformations: black dashed lines, gggg; gray dashed line, gg$\bar{g}\bar{g}$; gray continuous line, ggg$\bar{g}$; and long dashed black line, g$\bar{g}$gg$\bar{g}$.

to allow atoms of certain sizes to enter the cavity. In the structure of **1**, the carbon atoms at the bottom of the phenyl rings on opposite sides are 5.40 and 5.53 Å apart, and clearly any entering ion of the size of K^+ would need to push its way through these atoms and move the phenyl rings farther apart. After this was done, the rings would come together again, such that in the **1**·K^+ structure the distances between these atoms are 5.51 and 5.49 Å.

Conclusion

Calix[4]tubes represent an exciting new class of readily synthesized ionophores with exceptional selectivity for potassium over all group I metal cations and barium. A number of novel symmetric and asymmetric calix[4]tubes have been synthesized featuring a variety of upper rim substituents on the calix[4]arene units. The structural reorganization on binding offers a simple tool for evaluation of metal cation uptake in solution. ^{1}H NMR studies show the rate of complexation to be slow, which, combined with mass spectral evidence for potassium selectivity, suggests that calix[4]tubes have spherand-like[33] characteristics. The rate of complexation depends on the nature of the upper rim substituent, suggesting an axial route of entry, although the relative rates are difficult to rationalize. Molecular modeling simulations, based on crystallographic determinations, demonstrate that the most likely route of entry of the cation is axially through the selectivity filter of the calix[4]arene annuli and that the rate of entry can be related to the original torsion angles of the oxygen donor array and its ease of rearrangement to accommodate the potassium cation.

Experimental Section

All chemicals were commercial grade and used without further purification unless otherwise stated. Solvents were predried, purified by distillation, and stored under nitrogen where appropriate. Xylene was stored over calcium hydride, and triethylamine was distilled from potassium hydroxide.

Nuclear magnetic resonance spectra were recorded using either a 300 MHz Varian VXWorks spectrometer or a 500 MHz Varian Unity

(33) Cram, D. J.; Kaneda, T.; Helgeson, R. C.; Brown, S. B.; Knobler, C. B.; Maverick, E. F.; Trueblood, K. N. *J. Am. Chem. Soc.* **1985**, *107*, 3645−3657.

spectrometer. FAB mass spectral analyses were carried out by the EPSRC mass spectrometry service of University College, Swansea. Electrospray mass spectra were recorded using Micromass LCT equipment and MALDI on a Micromass TofSpec 2E Reflectron MALDI MS. Microanalyses were obtained from an elementar vario EL.[34] *p-tert*-Butylcalix[4]arene,[14] calix[4]arene,[15]1,3-*p-tert*-butylcalix[4]arene,[16] *p-tert*-octylcalix[4]arene,[17] *p*-isopropylcalix[4]arene,[18] and *p*-phenylcalix[4]-arene[19] were prepared according to the relevant literature procedures.

Tetrakis(2-hydroxyethoxy)-*p-tert*-octylcalix[4]arene (11). Three grams (2.5 mmol) of tetraethyl-*p-tert*-octylcalix[4]arene tetraacetate in diethyl ether (60 mL) was added dropwise to a cooled suspension of $LiAlH_4$ (760 mg, 20 mmol) in diethyl ether (60 mL) under nitrogen. The resulting suspension was allowed to warm to room temperature and stirred for 6 h. The suspension was cooled, and 1 N HCl (50 mL) was added slowly. The organic layer was separated and the aqueous layer washed with chloroform. The combined organic fractions were washed with brine and dried. Evaporation of the solvent and recrystallization of the residue from ethanol gave the title compound as a white solid (2.1 g, 83%). ^{1}H NMR (500 MHz, [D]$CHCl_3$, 18 °C): δ = 0.65 (s, 36H; (CH_3)$_3$), 1.10 (s, 24H; (CH_3)$_2$), 1.51 (s, 8H; $CHCH_2$), 3.20 (d, ^2J = 13 Hz (H, H), 4H; Ar−CH_2−Ar), 3.96 (m, 8H; CH_2OH), 3.99 (m, 8H; CH_2O), 4.36 (d, ^2J = 12.5 Hz (H, H), 4H; Ar−CH_2−Ar), 5.13 (t, ^3J = 5.5 Hz (H, H), 4H; O*H*), 6.84 (s, 8H; Ar−*H*). ^{13}C NMR (300 MHz, [D]$CHCl_3$, 18 °C): δ = 30.85 (Ar−CH_2−Ar), 31.30 ((CH_3)$_2$), 31.89 ((CH_3)), 32.58 (C(CH_3)$_3$), 38.14 (C(CH_3)$_2$), 57.57 (CH_2(CH_3)$_3$), 61.88 (OCH_2), 78.14 (HOCH_2), 126.52 (*Ar*−H), 133.39 (*Ar*−CH_2), 145.20 (*Ar*−C), 152.64 (*Ar*−O). MS (FAB): *m*/*z* 1072 [M + Na]. Anal. Calcd for $C_{68}H_{104}O_2$ (278.2): C, 77.82; H, 9.99. Found: C, 77.81; H, 9.93.

Tetrakis[(4-methylphenyl)sulfonyloxyethoxy]-*p-tert*-octylcalix[4]-arene (12). A 2.6 g (13.76 mmol) amount of *p*-toluenesulfonyl chloride was added to a solution of 1.8 g of tetrakis(2-hydroxyethoxy)-*p-tert*-octylcalix[4]arene in dichloromethane at 0 °C. Triethylamine (6 mL) was added, and the solution was stirred for 18 h. The solution was washed with 1 N HCl and brine and then dried. Evaporation of the solvent yielded a crude product which was purified by crystallization from dichloromethane/ethanol to give the desired compound as a white solid (2.5 g, 86%). ^{1}H NMR (500 MHz, [D]$CHCl_3$, 18 °C): δ = 0.64 (s, 36H; (CH_3)$_3$), 1.05 (s, 24H; (CH_3)$_2$), 1.49 (s, 8H; $CHCH_2$), 2.43 (s, 12H; Ar−CH_3), 2.99 (d, ^2J = 13 Hz (H, H), 4H; Ar−CH_2−Ar), 4.07 (t, ^3J = 5 Hz (H, H), 8 Hz; ArOCH_2), 4.23 (d, ^2J = 13 Hz (H, H), 4H; Ar−CH_2−Ar), 4.36 (t, ^3J = 5 Hz (H, H), 8 Hz; SO_3CH_2), 6.70 (s, 8H; Ar−*H*), 7.37 (d, ^3J = 8 Hz (H, H), 8H, tosyl 2,4), 7.83 (d, ^3J = 8 Hz (H, H), 8H, tosyl 3,5). ^{13}C NMR (75 MHz, [D]$CHCl_3$, 18 °C): δ = 21.91 (CH_3 (tosyl)), 31.42 ((CH_3)$_2$ + (C(CH_3)$_3$), 31.97 ((CH_3)$_3$), 32.53 (Ar-CH_2−Ar), 38.02 (C(CH_3)$_2$) 57.42 (CH_2(CH_3)$_3$), 69.47 (SO_3CH_2), 71.91 (OCH_2), 126.25 (*Ar*−H), 128.22 (tosyl 2,4), 130.18 (tosyl 3,5), 133.23 (*Ar*−S), 133.33 (*Ar*−CH_2), 144.68 (*Ar*−CH_3), 145.02 (*Ar*−C), 152.30 (*Ar*−O).

Calix[4]tube 1. A suspension of *p-tert*-butylcalix[4]arene (451 mg, 0.70 mmol) and K_2CO_3 (480 mg, 3.5 mmol) was stirred at room temperature for 2 h in acetonitrile (100 mL). Tetrakis[(4-methylphenyl)-sulfonyloxyethoxy]-*p-tert*-butylcalix[4]arene (1.0 g, 0.70 mmol) was added and the reaction mixture heated at reflux for 5 days. The solvent was then removed by evaporation and the residue resuspended in a 1:1 ethanol−water mixture. After heating at reflux overnight, the mixture was hot filtered and the crude product dissolved in chloroform (50 mL). The solution was filtered through paper with care, and then acetone (40 mL) was added. Filtration of the resulting microcrystaline solid gave calix[4]tube **1** in 51% yield. ^{1}H NMR (300 MHz, [D]$CHCl_3$, 18 °C): δ = 0.82 (s, 36H; (CH_3)$_3$), 1.32 (s, 36H; (CH_3)$_3$′), 3.26 (d, ^2J = 13 Hz (H, H), 8H; Ar−CH_2−Ar), 4.41 (s, 8H; OCH_2), 4.58 (d, ^2J = 13 Hz (H, H), 8H; Ar−CH_2−Ar), 5.16 (s, 8H; OCH_2′), 6.50 (s, 8H; Ar−*H*), 7.10 (s, 8H; Ar−*H*′); ^{13}C NMR (75 MHz, [D]$CHCl_3$, 18 °C): δ = 31.25 ((CH_3)$_3$), 31.96 ((CH_3)′), 32.62 (Ar−CH_2−Ar), 33.77 (C(CH_3)$_3$), 34.30 (C(CH_3)$_3$′), 72.71 (OCH_2), 73.21 (OCH_2′), 125.00 (Ar−H), 125.70 (*Ar*−H′), 132.14 (*Ar*−CH_2), 135.36 (*Ar*−CH_2′), 144.52 (*Ar*−CH), 144.76 (*Ar*−CH′), 153.08 (*Ar*−O), 156.23 (*Ar*−O′). ^{1}H NMR (500 MHz, [D]$CHCl_3$ + KI, 18 °C): δ = 1.08 (s, 72H; (CH_3)$_3$), 3.47 (d, ^2J = 13 Hz, 8H; Ar−CH_2−Ar), 4.46 (m, 16H; OCH_2), 4.60 (d, ^2J = 12 Hz, 8H; Ar−CH_2−Ar), 7.14 (s, 16H, Ar−*H*). MS (FAB): *m*/*z* 1401 [M + H]. Anal. Calcd for $C_{96}H_{120}O_8$ (1400): C, 82.24; H, 8.63. Found: C, 82.08; H, 9.20.

General Method for the Synthesis of Calix[4]tubes 2−8. A suspension of a tetrakis[(4-methylphenyl)sulfonyloxyethoxy]calix[4]-arene (1 mmol), a *para*-substituted calix[4]arene (1 mmol), and K_2CO_3 (690 mg, 5 mmol) in xylene (50 mL) was heated at reflux for 2−4 days. The mixture was cooled, and the solvent was removed by evaporation. The residue was then dissolved in a mixture of chloroform and water. The organic layer was separated, washed with water and brine, and then dried. Hot trituration of the residue with dichloromethane/ethanol yielded the calix[4]tube as a white solid.

Calix[4]tube 2. Yield: 67%. ^{1}H NMR (300 MHz, [D]$CHCl_3$, 18 °C): δ = 0.60 (s, 36H; (CH_3)$_3$), 0.82 (s, 36H; (CH_3)$_3$′), 0.83 (s, 24H; (CH_3)$_2$), 1.37 (s, 32H; (CH_3)$_2$′ + $CHCH_2$), 1.77 (s, 8H; $CHCH_2$′), 3.25 (d, ^2J = 13 Hz (H, H), 8H; Ar−CH_2−Ar), 4.34 (s, 8H; OCH_2), 4.61 (d, ^2J = 12 Hz (H, H), 8H; Ar−CH_2−Ar), 5.18 (s, 8H; OCH_2′), 6.51 (s, 8H; Ar−H), 7.09 (s, 8H; Ar−H′). ^{13}C NMR (75 MHz, [D]$CHCl_3$, 18 °C): δ = 30.84 ((CH_3)$_2$), 31.59 ((CH_3)$_3$), 31.83 ((CH_3)$_2$′), 32.23 (CH(CH_3)$_3$ + (CH_3)$_3$′), 32.40 (CH(CH_3)$_3$′), 32.76 (Ar−CH_2−Ar), 37.55 (CH(CH_3)$_2$), 38.06 (CH(CH_3)$_2$′), 56.78 (CH_2CH′), 57.20 (CH_2CH), 72.96 (OCH_2), 73.07 (OCH_2′), 125.61 (Ar−H), 126.31 (Ar−H′), 131.46 (Ar−CH_2), 134.82 (Ar−CH_2′), 143.47 (Ar−CH′), 143.70 (Ar−CH), 153.23 (Ar−O), 156.25 (Ar−O′). ^{1}H NMR (500 MHz [D]$CHCl_3$ + KI, 18 °C): δ = 0.39 (s 72H; (CH_3)$_3$), 1.11 (s, 48H; (CH_3)$_2$), 1.42 (s, 16H; $CHCH_2$), 3.40 (d, ^2J = 13 Hz, 8H; Ar−CH_2−Ar), 4.44 (s, 16H; OCH_2), 4.60 (d, ^2J = 12 Hz, 8H; Ar−CH_2−Ar), 7.05 (s, 16H, Ar−H). MS (MALDI): *m*/*z* 1889.33 [M + K]. Anal. Calcd for $C_{128}H_{184}O_8$ (1848): C, 83.06; H, 10.02. Found: C, 82.16; H, 9.76.

Calix[4]tube 3. Yield: 10%. ^{1}H NMR (500 MHz, [D]$CHCl_3$, 18 °C): δ = 3.35 (d, ^2J = 13 Hz (H, H), 8H; Ar−CH_2−Ar), 4.48 (s, 8H; OCH_2), 4.60 (d, ^2J = 13 Hz (H, H), 8H; Ar−CH_2−Ar), 5.18 (s, 8H; OCH_2′), 6.42 (t, ^3J = 8 Hz (H, H), 4H; Ar−H_{para}), 6.49 (d, ^3J = 8 Hz (H, H), 8H; Ar−H_{ortho}), 6.93 (t, ^3J = 8 Hz (H, H), 4H; Ar−H_{para}′), 7.18 (d, ^3J = 8 Hz (H, H) 8H; Ar−H_{ortho}′). ^{13}C NMR (75 MHz, [D]-$CHCl_3$, 18 °C): δ = 31.99 (Ar−CH_2−Ar), 72.19 (OCH_2), 72.02 (OCH_2′), 122.30 (Ar−$H_{(para)}$′), 122.561 (*Ar*−$H_{(para)}$), 128.19 (Ar−$H_{(meta)}$), 129.01 (*Ar*−$H_{(meta)}$′), 132.88 (*Ar*−CH_2), 136.07 (*Ar*−CH_2′), 154.75 (*Ar*−O), 158.74 (*Ar*−O ′). MS (MALDI): *m*/*z* 975.94 [M + Na]. Anal. Calcd for $C_{64}H_{56}O_8$ (952): C, 80.64; H, 5.93. Found: C, 80.71; H, 6.52.

Calix[4]tube 4. Yield: 66% tetrakis[(4-methylphenyl)sulfonyloxy-ethoxy]-*p-tert*-butylcalix[4]arene and calix[4]arene; 10% tetrakis[(4-methylphenyl)sulfonyloxyethoxy]calix[4]arene and *p-tert*-butylcalix-[4]arene. ^{1}H NMR (300 MHz, [D]$CHCl_3$, 18 °C): δ = 0.83 (s, 18H; (CH_3)$_3$), 1.33 (s, 18H; (CH_3)$_3$′), 3.29 (d, ^2J = 11 Hz (H, H), 4H; Ar−CH_2−Ar (*t*-Bu)), 3.33 (d, ^2J = 13 Hz (H, H), 4H; Ar−CH_2−Ar (*p*-H)), 4.48 (s, 8H; OCH_2), 4.57 (d, ^2J = 13 Hz (H, H), 4H; Ar−CH_2−Ar (*t*-Bu′)), 4.63 (d, ^2J = 13 Hz (H, H), 4H; Ar−CH_2−Ar (*p*-H)′), 5.17 (m, 8H; OCH_2′), 6.40 (m, 2H; Ar−*H* (*p*-H_{para})), 6.45 (m, 4H; Ar−*H* (*p*-H_{ortho})), 6.53 (s, 4H; Ar−*H*), 6.88 (t, ^2J = 7 Hz (H, H), 2H; Ar−*H* (*p*-H_{para})′), 7.12 (m, 4H; Ar−*H* (*p*-H_{ortho})), 7.14 (s, 4H; Ar−*H*′). ^{13}C NMR (75 MHz, [D]$CHCl_3$, 18 °C): δ = 30.99 ((CH_3)$_3$), 31.71 ((CH_3)$_3$′), 32.13 (Ar−CH_2−Ar (*p*-H)), 32.13 (Ar−CH_2−Ar (*t*-Bu)), 33.56 (CH(CH_3)$_3$), 34.10 (CH(CH_3)$_3$′), 72.31 (OCH_2), 72.36 (OCH_2),

(34) Problems associated with microanalysis of calixarenes have previously been reported: (a) Böhmer, V.; Jung, K.; Schön, M.; Wolff, A. *J. Org. Chem.* **1992**, *57*, 790−792. (b) Gutsche, C. D.; See, K. A. *J. Org. Chem.* **1992**, *57*, 4527−4539.
(35) Bain, A. D.; Cramer, J. A. *J. Magn. Reson. A* **1996**, *118*, 21−27.
(36) Kabsch, W. *J. Appl. Crystallogr.* **1988**, *21*, 916−924.
(37) Sheldrick, G. M. Shelx86. *Acta Crystallogr.* **1990**, *A46*, 467−473.
(38) Sheldrick, G. M. Shelxl, program for crystal structure refinement, University of Gottingen, 1993.

72.83 (O*C*H$_2$ (*p*-H)′), 73.06 (O*C*H$_2$ (*t*-Bu)′), 122.11 (*Ar*−H$_{(para)}$ (*p*-H)′), 122.52 (*Ar*−H$_{(para)}$ (*p*-H)), 124.90 (*Ar*−H (*t*-Bu)), 125.54 (*Ar*−H (*t*-Bu)′), 128.07 (*Ar*−H$_{(meta)}$ (*p*-H)), 128.94 (*Ar*−H$_{(meta)}$ (*p*-H)′), 131.78 (*Ar*−CH$_2$ (*t*-Bu)), 133.03 (*Ar*−CH$_2$ (*p*-H)), 135.16 (*Ar*−CH$_2$ (*t*-Bu)′), 136.12 (*Ar*−CH$_2$ (*p*-H)′), 144.40 (*Ar*−C (*t*-Bu)), 144.80 (*Ar*−C (*t*-Bu)′), 152.63 (*Ar*−O (*t*-Bu)), 154.99 (*Ar*−O (*p*-H)), 156.07 (*Ar*−O (*t*-Bu)′), 158.61 (*Ar*−O (*p*-H)′). ^{1}H NMR (500 MHz, [D]CHCl$_3$ + KI, 18 °C): δ = 1.05 (s 36H; (C*H*$_3$)$_3$ (*t*-Bu)), 3.46 (d, ^2J = 12 Hz, 4H; Ar−C*H*$_2$−Ar), 3.45 (d, ^2J = 13 Hz, 4H; Ar−C*H*$_2$−Ar), 4.34 (s, 16H; OC*H*$_2$), 4.58 (d, ^2J = 13 Hz, 4H; Ar−C*H*$_2$−Ar), 4.62 (d, ^2J = 13 Hz, 4H; Ar−C*H*$_2$−Ar), 6.81 (t, ^3J = 8 Hz, 4H; Ar−*H* (*p*-H$_{para}$)), 7.12 (s, 8H, Ar−*H* (*t*-Bu)), 7.13 (d, ^3J = 8 Hz, 8H; Ar−*H* (*p*-H$_{ortho}$)). MS (FAB): *m*/*z* 1178 [M + H]. Anal. Calcd for $C_{80}H_{88}O_8$ (1176): C, 81.60; H, 7.53. Found: C, 81.18; H, 7.98.

Calix[4]tube 5. Yield: 67% tetrakis[(4-methylphenyl)sulfonyloxyethoxy]-*p-tert*-butylcalix[4]arene and *p-tert*-octylcalix[4]arene. ^{1}H NMR (300 MHz, [D]CHCl$_3$, 18 °C): δ = 0.59 (s, 18H; (C*H*$_3$)$_3$ (*t*-Oct)), 0.80 (s, 18H; (C*H*$_3$)$_3$ (*t*-Oct)′), 0.82 (s, 12H; (C*H*$_3$)$_2$ (*t*-Oct)), 0.83 (s, 18H; (C*H*$_3$)$_3$ (*t*-Bu)), 1.33 (s, 22H; (C*H*$_3$)$_3$ (*t*-Bu)′ + CHC*H*$_2$ (*t*-Oct)), 1.35 (s, 12H, (C*H*$_3$)$_2$ (*t*-Oct)′), 1.78 (s, 4H; CHC*H*$_2$ (*t*-Oct)′), 3.24 (d, ^2J = 12 Hz (H, H), 4H; Ar−C*H*$_2$−Ar (*t*-Oct)), 3.28 (d, ^2J = 13 Hz (H, H), 4H; Ar−C*H*$_2$−Ar (*t*-Bu)), 4.37 (m, 8H; OC*H*$_2$), 4.58 (d, ^2J = 13 Hz (H, H), 4H; Ar−C*H*$_2$−Ar (*t*-Oct)′), 4.61 (d, ^2J = 13 Hz (H, H), 4H; Ar−C*H*$_2$−Ar (*t*-Bu)′), 5.17 (m, 8H; OC*H*$_2$′), 6.48 (s, 4H; Ar−*H* (*t*-Oct)), 6.52 (s, 4H; Ar−*H* (*t*-Bu)), 7.06 (s, 4H; Ar−*H* (*t*-Oct)′), 7.14 (s, 4H; Ar−*H* (*t*-Bu)′). ^{13}C NMR (75 MHz, [D]CHCl$_3$, 18 °C): δ = 31.09 ((*C*H$_3$)$_2$ (*t*-Oct)), 31.27 ((*C*H$_3$)$_3$ (*t*-Oct)′), 31.89 ((*C*H$_3$)$_3$ (*t*-Oct)), 31.97 ((*C*H$_3$)$_3$ (*t*-Bu)), 32.31 ((*C*H$_3$)$_2$ (*t*-Oct)′), 32.45 (*C*H(CH$_3$)$_3$), 32.49 ((*C*H$_3$)$_3$ (*t*-Bu) + Ar−*C*H$_2$−Ar (*t*-Bu)), 32.62 ((*C*H$_3$)$_3$ (*t*-Bu)′), 33.04 (Ar−*C*H$_2$−Ar (*t*-Oct)), 33.79 (*C*H(CH$_3$)$_3$ (*t*-Bu)), 34.33 (*C*H(CH$_3$)$_3$ (*t*-Bu)′), 37.76 (*C*H(CH$_3$)$_2$ (*t*-Oct)), 38.23 (*C*H(CH$_3$)$_2$ (*t*-Oct)′), 56.89 (*C*H$_2$CH (*t*-Oct)′), 57.51 (*C*H$_2$CH (*t*-Oct)), 72.87 (O*C*H$_2$ (*t*-Bu)), 73.09 (O*C*H$_2$ (*t*-Oct)), 73.18 (O*C*H$_2$ (*t*-Bu)′), 73.36 (O*C*H$_2$ (*t*-Oct)′), 125.00 (*Ar*−H (*t*-Bu)), 125.72 (*Ar*−H (*t*-Bu)′), 125.89 (*Ar*−H (*t*-Oct)), 126.67 (*Ar*−H (*t*-Oct)′), 131.69 (*Ar*−CH$_2$ (*t*-Oct)), 132.15 (*Ar*−CH$_2$ (*t*-Bu)), 134.99 (*Ar*−CH$_2$ (*t*-Oct)′), 135.49 (*Ar*−CH$_2$ (*t*-Bu)′), 143.60 (*Ar*−C (*t*-Oct)′), 143.64 (*Ar*−C (*t*-Oct)), 144.54 (*Ar*−C (*t*-Bu)), 144.80 (*Ar*−C (*t*-Bu)′), 153.08 (*Ar*−O (*t*-Bu)), 153.49 (*Ar*−O (*t*-Oct)), 156.32 (*Ar*−O (*t*-Oct)′), 156.42 (*Ar*−O (*t*-Bu)′). ^{1}H NMR (500 MHz, [D]CHCl$_3$ + KI, 18 °C): δ = 0.39 (s 36H; (C*H*$_3$)$_3$ (*t*-Oct)), 0.05 (s, 36H; (C*H*$_3$)$_3$ (*t*-Bu)), 11.12 (s, 24H; (C*H*$_3$)$_2$ (*t*-Oct)), 1.42 (s, 8H; *C*HCH$_2$ (*t*-Oct)), 3.43 (d, ^2J = 11 Hz, 8H; Ar−C*H*$_2$−Ar), 4.40 (s, 8H; OC*H*$_2$), 4.47 (s, 8H; OC*H*$_2$), 4.58 (d, ^2J = 12 Hz, 4H; Ar−C*H*$_2$−Ar), 4.59 (d, ^2J = 13 Hz, 4H; Ar−C*H*$_2$−Ar), 7.05 (s, 8H, Ar−*H*), 7.11 (s, 8H, Ar−*H*). MS (MALDI): *m*/*z* 1649.27 [M + Na]. Anal. Calcd for $C_{112}H_{152}O_8$ (1624): C, 82.71; H, 9.42. Found: C, 82.17; H, 9.79.

Calix[4]tube 6. Yield: 58% tetrakis[(4-methylphenyl)sulfonyloxyethoxy]-*p-tert*-butylcalix[4]arene and *p*-isopropylcalix[4]arene. ^{1}H NMR (300 MHz, [D]CHCl$_3$, 18 °C): δ = 0.73 (d, ^3J = 7 Hz (H, H), 12H; CH(C*H*$_3$) (isop)), 0.80 (s, 18H; (C*H*$_3$)$_3$ (*t*-Bu)), 1.24 (d, ^3J = 7 Hz (H, H), 12H; CH(C*H*$_3$) (isop)′), 1.30 (s, 18H; (C*H*$_3$)$_3$ (*t*-Bu)′), 2.24 (sep, ^3J = 7 Hz (H, H) 2H; C*H*(CH$_3$)$_2$ (isop)), 2.84 (sep, ^3J = 7 Hz (H, H) 2H; C*H*(CH$_3$)$_2$ (isop)′), 3.22 (d, ^2J = 13 Hz (H, H), 4H; Ar−C*H*$_2$−Ar (isop)), 3.24 (d, ^2J = 13 Hz (H, H), 4H; Ar−C*H*$_2$−Ar (*t*-Bu)), 4.40 (s, 8H; OC*H*$_2$), 4.54 (d, ^2J = 13 Hz (H, H), 4H; Ar−C*H*$_2$−Ar (isop)′), 4.55 (d, ^2J = 13 Hz (H, H), 4H; Ar−C*H*$_2$−Ar (*t*-Bu)′) 5.08 (m, 4H; OC*H*$_2$ (isop)′), 5.12 (m, 4H; OC*H*$_2$ (*t*-Bu)′), 6.24 (s, 4H; Ar−*H* (isop)), 6.48 (s, 4H; Ar−*H* (*t*-Bu), 6.92 (s, 4H; Ar−*H* (isop)′), 7.10 (s, 4H; Ar−*H* (*t*-Bu)′). ^{13}C NMR (75 MHz, [D]CHCl$_3$, 18 °C): δ = 23.50 ((*C*H$_3$)$_2$ (isop)), 24.50 ((*C*H$_3$)$_2$ (isop)′), 30.99 ((*C*H$_3$)$_3$ (*t*-Bu)), 31.71 ((*C*H$_3$)$_2$ (*t*-Bu)′), 32.22 (Ar−*C*H$_2$−Ar (*t*-Bu) + (isop)), 32.45 (*C*H(CH$_3$)$_2$ (isop)), 33.53 (*C*H(CH$_3$)$_3$ (*t*-Bu)), 33.65 (*C*H(CH$_3$)$_2$ (isop)′), 34.07 (*C*H-(CH$_3$)$_3$ (*t*-Bu)′), 72.27 (O*C*H$_2$), 72.38 (O*C*H$_2$), 72.96 (O*C*H$_2$ (*t*-Bu)′ + (isop)′), 124.80 (*Ar*−H (*t*-Bu)′), 125.47 (*Ar*−H (*t*-Bu)′), 125.73 (*Ar*−H (isop)), 126.49 (*Ar*−CH (isop)′), 131.83 (*Ar*−CH$_2$ (*t*-Bu)), 132.52 (*Ar*−CH$_2$ (isop)), 135.15 (*Ar*−CH$_2$ (*t*-Bu)′), 135.63 (*Ar*−CH$_2$ (isop)′), 141.88 (*Ar*−C (isop)), 142.30 (*Ar*−C (isop)′), 144.23 (*Ar*−C (*t*-Bu)), 144.55 (*Ar*−C (*t*-Bu)′), 152.76 (*Ar*−O (*t*-Bu)), 153.04 (*Ar*−O (isop)), 156.09 (*Ar*−O (*t*-Bu)′), 156.41 (*Ar*−O (isop)′). ^{1}H NMR (500 MHz [D]CHCl$_3$ + KI, 18 °C): δ = 0.98 (d, ^3J = 7 Hz, 24H; ((C*H*$_3$)$_2$ (isop)), 1.06 (s 36H; (C*H*$_3$)$_3$ (*t*-Bu)),), 2.61 (sep, ^3J = 7 Hz (H, H) 4H; C*H*(CH$_3$)$_2$ (isop)), 3.44 (d, ^2J = 12 Hz, 4H; Ar−C*H*$_2$−Ar), 3.45 (d, ^2J = 13 Hz, 4H; Ar−C*H*$_2$−Ar), 4.34 (s, 16H; OC*H*$_2$), 4.56 (d, ^2J = 12 Hz, 4H; Ar−C*H*$_2$−Ar), 4.57 (d, ^2J = 12 Hz, 4H; Ar−C*H*$_2$−Ar), 6.96 (s, 8H, Ar−*H*), 7.12 (s, 8H, Ar−*H*). MS (FAB): *m*/*z* 1343 [M − 2H]. Anal. Calcd for $C_{92}H_{108}O_8$ (1344): C, 82.35; H, 8.11. Found: C, 80.80; H, 8.06.

Calix[4]tube 7. Yield: 51% tetrakis[(4-methylphenyl)sulfonyloxyethoxy]-*p-tert*-butylcalix[4]arene and *p*-phenylcalix[4]arene. ^{1}H NMR (300 MHz, [D]CHCl$_3$, 18 °C): δ = 0.83 (s, 18H; (C*H*$_3$)$_3$), 1.33 (s, 18H; (C*H*$_3$)$_3$′), 3.31 (d, ^2J = 13 Hz (H, H), 4H; Ar−C*H*$_2$−Ar (*t*-Bu)), 3.46 (d, ^2J = 13 Hz (H, H), 4H; Ar−C*H*$_2$−Ar (phenyl)) 4.51 (m, 8H; OC*H*$_2$), 4.60 (d, ^2J = 13 Hz (H, H), 4H; Ar−C*H*$_2$−Ar (*t*-Bu)), 4.73 (d, ^2J = 13 Hz (H, H), 4H; Ar−C*H*$_2$−Ar (phenyl)), 5.11 (m, 4H; OC*H*$_2$ (*t*-Bu)′), 5.33 (m, 4H, OC*H*$_2$ (phenyl)′), 6.54 (s, 4H; Ar−*H* (*t*-Bu)), 6.62 (s, 4H; Ar−*H* (phenyl)), 6.75 (m, 4H; *o*-Ar−*H* (phenyl), 6.97 (m, 6H; *m*,*p*-Ar−*H* (phenyl)), 7.15 (s, 4H; Ar−*H* (*t*-Bu)′), 7.31 (t, ^2J = 8 Hz (H, H), 2H; *p*-Ar−*H* (phenyl)′), 7.40 (s, 4H; Ar−*H* (phenyl)′), 7.44 (t, ^3J = 7 Hz 4H; *m*-Ar−*H* (phenyl)′), 7.12 (m, 4H; *o*-Ar−*H* (phenyl)′). ^{13}C NMR (75 MHz, [D]CHCl$_3$, 18 °C): δ = 31.24 ((*C*H$_3$)$_3$), 31.96 ((*C*H$_3$)$_2$′), 32.44 (Ar−*C*H$_2$−Ar (*t*-Bu)), 32.76 (Ar−*C*H$_2$−Ar (phenyl)), 33.80 (*C*H(CH$_3$)$_3$), 34.35 (*C*H(CH$_3$)$_3$′), 72.55 (O*C*H$_2$), 72.67 (O*C*H$_2$), 73.04 (O*C*H$_2$ (*t*-Bu)′), 73.52 (O*C*H$_2$ (phenyl)′), 125.19 (*Ar*−H (*t*-Bu)), 125.81 (*Ar*−H (*t*-Bu)′), 126.19 (*p*-*Ar*−H (phenyl)′) 126.79 (*p*-*Ar*−H (phenyl)′) 126.97 (*o*-*Ar*−H (phenyl)), 127.34 (*o*-*Ar*−H (phenyl)′), 127.45 (*Ar*−H (phenyl)), 127.93 (*Ar*−H (phenyl)′), 128.34 (*m*-*Ar*−H (phenyl)),128.85 (*m*-*Ar*−H (phenyl)′), 132.02 (*Ar*−CH$_2$ (*t*-Bu)), 133.37 (*Ar*−CH$_2$ (phenyl)), 135.39 (*Ar*−CH$_2$ (*t*-Bu)′ + O−*Ar*−Ar (phenyl)), 136.34 (O−*Ar*−Ar (phenyl)′), 136.53 (*Ar*−CH$_2$ (phenyl)′), 141.39 (*Ar*−Ar−O (phenyl)), 141.62 (*Ar*−Ar−O (phenyl)′), 144.68 (*Ar*−C (*t*-Bu)), 145.11 (*Ar*−C (*t*-Bu)′), 152.83 (*Ar*−O (*t*-Bu)), 154.91 (*Ar*−O (phenyl)), 156.30 (*Ar*−O (*t*-Bu)′), 158.51 (*Ar*−O (phenyl)′). MS (FAB): *m*/*z* 1505.04 [M + Na]. Anal. Calcd for $C_{104}H_{104}O_8$ (1480): C, 84.29; H, 7.07. Found: C, 82.40; H, 7.62.

Calix[4]tube 8. Yield: 61% tetrakis[(4-methylphenyl)sulfonyloxyethoxy]-*p-tert*-octylcalix[4]arene and calix[4]arene; 20% tetrakis[(4-methylphenyl)sulfonyloxyethoxy]calix[4]arene and *p-tert*-octylcalix-[4]arene. ^{1}H NMR (300 MHz, [D]CHCl$_3$, 18 °C): δ = 0.59 (s, 18H; (C*H*$_3$)$_3$), 0.82 (s, 18H; (C*H*$_3$)$_3$′), 0.83 (s, 12H; (C*H*$_3$)$_2$), 1.36 (s, 16H; (C*H*$_3$)$_2$′ + CHC*H*$_2$), 1.77 (s, 4H; CHC*H*$_2$′), 3.26 (d, ^2J = 13 Hz (H, H), 4H; Ar−C*H*$_2$−Ar (*t*-Oct)), 3.33 (d, ^2J = 13 Hz (H, H), 4H; Ar−C*H*$_2$−Ar (*p*-H)), 4.41 (m, 8H; OC*H*$_2$), 4.56 (d, ^2J = 13 Hz (H, H), 4H; Ar−C*H*$_2$−Ar (*t*-Oct)′), 4.64 (d, ^2J = 13 Hz (H, H), 4H; Ar−C*H*$_2$−Ar (*p*-H)′), 5.18 (m, 8H; OC*H*$_2$′), 6.39 (m, 2H; Ar−*H* (*p*-H$_{para}$)), 6.47 (m, 4H; Ar−*H* (*p*-H$_{ortho}$)), 6.51 (s, 8H; Ar−*H*), 6.90 (t, ^2J = 7 Hz (H, H), 2H; Ar−*H* (*p*-H$_{para}$)′), 7.09 (s, 8H; *Ar*−H′), 7.16 (d, ^2J = 7 Hz (H, H), 4H; *Ar*−H (*p*-H$_{ortho}$)′). ^{13}C NMR (75 MHz, [D]CHCl$_3$, 18 °C): δ = 30.86 ((*C*H$_3$)$_2$), 31.56 ((*C*H$_3$)$_3$), 31.83 ((*C*H$_3$)$_2$′), 32.06 (Ar−*C*H$_2$−Ar (*p*-H)), 32.19 ((*C*H$_3$)$_3$′), 32.24 (*C*H(CH$_3$)$_3$), 32.40 (*C*H(CH$_3$)$_3$′), 32.63 (Ar−*C*H$_2$−Ar (*t*-Oct)), 37.53 (*C*H(CH$_3$)$_2$), 38.07 (*C*H(CH$_3$)$_2$′), 56.76 (C*H*$_2$CH′), 57.20 (C*H*$_2$CH), 72.52 (O*C*H$_2$), 72.69 (O*C*H$_2$), 72.83 (O*C*H$_2$′), 73.29 (O*C*H$_2$′), 122.12 (*Ar*−H$_{(para)}$ (*p*-H), 122.55 (*Ar*−H$_{(para)}$ (*p*-H), 125.74 (*Ar*−H (*t*-Oct)), 126.36 (*Ar*−H (*t*-Oct)′), 128.07 (*Ar*−H$_{(meta)}$ (*p*-H)), 128.94 (*Ar*−H$_{(meta)}$ (*p*-H)′), 131.35 (*Ar*−CH$_2$ (*t*-Oct)), 133.00 (*Ar*−CH$_2$ (*p*-H)), 134.73 (*Ar*−CH$_2$ (*t*-Oct)′), 136.18 (*Ar*−CH$_2$ (*p*-H)′), 143.48 (*Ar*−C (*t*-Oct)), 143.98 (*Ar*−C (*t*-Oct)′), 153.02 (*Ar*−O (*t*-Oct)), 154.98 (*Ar*−O (*p*-H)), 156.16 (*Ar*−O (*t*-Oct)′), 158.82 (*Ar*−O (*p*-H)′). ^{1}H NMR (500 MHz, [D]CHCl$_3$ + KI, 18 °C): δ = 0.39 (s, 36H; (C*H*$_3$)$_3$ (*t*-Oct)), 1.11 (s, 24H; (C*H*$_3$)$_2$ (*t*-Oct)), 1.42 (s, 8H; CHC*H*$_2$ (*t*-Oct)), 3.43 (d, ^2J = 13 Hz, 4H; Ar−C*H*$_2$−Ar), 3.47 (d, ^2J = 13 Hz, 4H; Ar−C*H*$_2$−Ar), 4.42 (s, 8H; OC*H*$_2$), 4.47 (s, 8H; OC*H*$_2$), 4.58 (d, ^2J = 13 Hz, 4H; Ar−C*H*$_2$−Ar), 4.63 (d, ^2J = 13 Hz, 4H; Ar−C*H*$_2$−

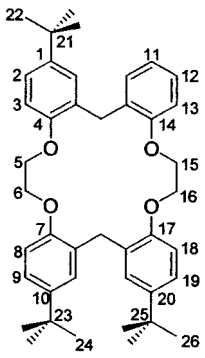

Figure 16. Numbering scheme for NMR assignments of calix[4]tube **9**.

Ar), 6.79 (t, ^3J = 8 Hz, 4H; Ar−*H* (*p*-H_{para})), 7.05 (s, 8H, Ar−*H* (*t*-Oct)), 7.11 (d, ^3J = 8 Hz, 8H; Ar−*H* (*p*-H_{ortho})). MS (MALDI): *m*/*z* 1425.01 [M + Na]. Anal. Calcd for $C_{96}H_{120}O_8$ (1400): C, 82.24; H, 8.63. Found: C, 82.18; H, 8.68.

Calix[4]tube 9. Yield: 53% tetrakis[(4-methylphenyl)sulfonyloxyethoxy]-*p*-*tert*-butylcalix[4]arene and 1,3-*p*-*tert*-butylcalix[4]arene. For numbering, see Figure 16 (refers to conformer B). ^{1}H NMR (500 MHz, [D]$CHCl_3$, 18 °C): δ = 0.81 (s, 18H; 26), 0.81 (s, 18H; 22′), 0.83 (s 18H; 24′), 1.31 (s, 18H; 24), 1.32 (s, 18H; 26′), 1.33 (s, 18H; 22), 3.26 (d, ^2J = 12 Hz (H, H), 4H; 28), 3.27 (d, ^2J = 12 Hz (H, H), 4H; 28′), 3.27 (d, ^2J = 13 Hz (H, H), 4H; 27), 3.28 (d, ^2J = 12 Hz (H, H), 4H; 27′), 4.39 (s, 8H; 5′ + 6′), 4.42 (s, 8H; 15 + 16), 4.55 (d, ^2J = 12 Hz (H, H), 4H; 28 + 28′), 4.58 (d, ^2J = 12 Hz (H, H), 4H; 27′), 4.59 (d, ^2J = 13 Hz (H, H), 4H; 27), 5.05 (m, 4H; 5), 5.13 (m, 4H; 16′), 5.18 (m, 4H; 6), 5.23 (m, 4H; 15′), 6.40 (m, 6H; 11 + 12), 6.48 (s, 4H; 9′), 6.50 (s, 8H; 2′ + 19), 6.83 (t, ^3J = 7.5 Hz (H, H), 2H; 11′), 7.07 (s, 4H; 2), 7.09 (d, ^3J = 7.5 Hz (H, H), 4H; 12′), 7.11 (s, 4H; 19′), 7.12 (s, 4H; 9). ^{13}C NMR (125 MHz, [D]$CHCl_3$, 18 °C): δ = 31.00 (22′ + 26), 31.14 (24′), 31.72 (24 + 26′), 31.74 (22), 32.21 (28′), 32.62 (27′ + 28), 32.51 (27), 33.54 (21′ + 25), 33.57 (23′), 34.08 (23 + 25′), 34.11 (21), 72.30 (15 + 16), 72.43 (5′ + 6′), 72.91 (5/6), 72.97 (16′ + 5/6), 73.02 (15′), 121.97 (11′), 122.38 (11), 124.08 (9′), 124.86 (2′ + 19), 125.50 (9 + 19′), 125.64 (2), 127.95 (12), 128.71 (12′), 131.76 (3′), 131.80 (8/8′/18/18′), 131.82 (8/8′/18/18′), 133.25 (13), 134.97 (3), 135.15 (8/8′/18/18′), 135.99 (13′), 144.31 (20), 144.32 (1′), 144.48 (1), 144.50 (10′), 144.65 (10 + 20′), 152.67 (17), 152.73 (7′), 152.91 (4′), 155.01 (14), 156.06 (17′), 156.15 (4 + 7), 158.49 (14′). ^{1}H NMR (500 MHz, [D]$CHCl_3$ + KI, 18 °C): δ = 1.04 (s, 18H; $(CH_3)_3$ (*t*-Bu)), 1.04 (s, 18H; $(CH_3)_3$ (*t*-Bu)), 1.07 (s, 18H; $(CH_3)_3$ (1,3-*t*-Bu)), 3.45 (d, ^2J = 13 Hz, 4H; Ar−CH_2−Ar), 3.51 (d, ^2J = 13 Hz, 4H; Ar−CH_2−Ar), 4.46 (s, 16H; OCH_2), 4.57 (d, ^2J = 13 Hz, 4H; Ar−CH_2−Ar), 4.60 (d, ^2J = 13 Hz, 4H; Ar−CH_2−Ar), 6.78 (t, ^3J = 7.5 Hz, 2H; *p*-H (1,3-*t*-Bu)), 7.09 (d, ^3J = 8 Hz, 4H, *mH* (1,3-*t*-Bu), 7.11 (s, 8H, Ar−*H* (*t*-Bu)), 7.12 (s, 4H, Ar−*H* (1,3-*t*-Bu)). MS (MALDI): *m*/*z* 1313.13 [M + Na], 1311 [M + Na]. Anal. Calcd for $C_{88}H_{104}O_8$: C, 81.95; H, 8.13. Found: C, 81.19; H, 8.14.

Acknowledgment. This work was supported by an EPSRC Postdoctoral Fellowship (S.E.M.). The University of Reading and the EPSRC are gratefully acknowledged for funding toward the crystallographic image plate system. The EPSRC Mass Spectrometry Service (University College, Swansea) is gratefully acknowledged for the provision of FAB mass spectra. V.F. thanks F.C.T. for a sabbatical leave grant.

Supporting Information Available: Tables giving the crystal data and structure refinement information, bond lengths and bond angles, atomic and hydrogen coordinates, and isotropic and anisotropic displacement coordinates for **2** (PDF). This material is available free of charge via the Internet at http://pubs.acs.org.

JA011856M